

Invited review

A brief review of the phase-field-based lattice Boltzmann method for multiphase flows

Huili Wang¹, Xiaolei Yuan², Hong Liang³, Zhenhua Chai²*[✉], Baochang Shi²

¹School of Mathematics and Computer Science, Wuhan Textile University, Wuhan 430073, P. R. China

²School of Mathematics and Statistics, Huazhong University of Science and Technology, Wuhan 430074, P. R. China

³Department of Physics, Hangzhou Dianzi University, Hangzhou 310018, P. R. China

Keywords:

Lattice Boltzmann method
phase-field model
multiphase flows

Cited as:

Wang, H., Yuan, X., Liang, H., Chai, Z., Shi, B. A brief review of the phase-field-based lattice Boltzmann method for multiphase flows. *Capillarity*, 2019, 2(3): 33-52, doi: 10.26804/capi.2019.03.01.

Abstract:

In this paper, we present a brief overview of the phase-field-based lattice Boltzmann method (LBM) that is a distinct and efficient numerical algorithm for multiphase flow problems. We first give an introduction to the mathematical theory of phase-field models for multiphase flows, and then present some recent progress on the LBM for the phase-field models which are composed of the classic Navier-Stokes equations and the Cahn-Hilliard or Allen-Cahn equation. Finally, some applications of the phase-field-based LBM are also discussed.

1. Introduction

The multiphase flows are universal and are of great importance in both nature and industrial processes, for instance, the fall of droplet (Gan et al., 2009), the recovery of crude oil (Li et al., 2005) and the design of microfluidic chip (Teh et al., 2008; Chen and Hu, 2015), which are also the key problems in the fields of the energy, environment and chemical engineering. The transport processes of the multiphase flows are very complicated due to the topological changes of the interface among different phases, including the migration, deformation, breakup and merging of the phase interface (Anna, 2016). The multiphase flow is a multi-field coupling problem (Brennen, 2005), and usually it is hard to obtain its exact solution with the analytical method (Cristini and Tan, 2004; Leshansky et al., 2012). In the past decades, the experimental method has been widely used to study the multiphase flow problems, and can also capture the macroscopic dynamic behavior of interface (Link et al., 2004; Jullien et al., 2009; Kintses et al., 2010), while it is difficult to accurately describe the details of the fluid flows (Wörner, 2012).

With the rapid development of computer technology, nu-

merical simulation has become an effective technique in the study of multiphase flows (Yue et al., 2004; Li et al., 2012). The current numerical methods for multiphase flow problems can be divided into two categories: the sharp-interface (Sun and Beckermann, 2007; Sussman et al., 2007) and the diffuse-interface approaches (Anderson et al., 1998; Jacqmin, 1999). The sharp-interface approach usually includes volume-of-fluid (VOF) (Hirt and Nichols, 1981; Bonhomme et al., 2012), level-set method (LSM) (Sussman et al., 1994; Smith et al., 2002) and front-tracking method (FTM) (Unverdi and Tryggvason, 1992; Muradoglu and Tasoglu, 2010). This type of approach requires solving the Navier-Stokes and interface tracking equations. The VOF method (Hirt and Nichols, 1981) does not directly track the motion of the interface particles, and the free surface depends on the volume fraction of the fluid in the grid unit. The VOF method can depict the topological change of complex interfaces, but most of the interface reconstruction formats have only first-order approximation, and the volume fraction function is discontinuous at the phase interface, which is easy to cause numerical oscillation. In addition, the VOF method is difficult to simply generalize to the three-dimensional case where a curved surface is usually

*Corresponding author.

E-mail address: hlwang@wtu.edu.cn (H. Wang); ximenchui.niu@163.com (X. Yuan); lianghongstefanie@163.com (H. Liang); hustczh@hust.edu.cn (Z. Chai); shibc@hust.edu.cn (B. Shi).

2652-3310 © The Author(s) 2019.

Received May 9, 2019; revised June 1, 2019; accepted June 2, 2019; available online June 7, 2019.

involved. Unlike the VOF method, in the LSM (Sussman et al., 1994), the motion of the phase interface is characterized by a continuous function (distance function), which is obtained through solving the transport equation. The zero level-set of the continuous function is the phase interface of different fluids. The advantage of LSM is that the the interface curvature, normal vector and surface tension can be easily calculated. However, for the multiphase flow problems which involve the large topological interface changes, the characteristics of the distance function would be not preserved in the computation of the continuous function, and for this reason, a re-distancing process is needed. However, the re-distancing process would lead to the fact that the mass conservation can not be satisfied. In the FTM (Unverdi and Tryggvason, 1992), the Lagrangian method is adopted to track the motion of each point on the fluid interface. Compared to the VOF and LSM, the FTM has a clear interface with high-order accuracy, and what is more, the surface tension and surface energy can be calculated directly and efficiently. However, the FTM would become difficult for multiphase flow problems with complex topological interface changes.

In the sharp-interface approach, the different fluids are separated by the sharp interface, thus the fluid properties (e.g., density, velocity and viscosity) at the interface are discontinuous. Different from the sharp-interface approach, the basic idea of the diffuse-interface approach is to replace the sharp interface with a thin but nonzero-thickness transitional region, where the physical quantities vary smoothly across the interface. In the diffuse-interface approach, it is also not necessary to explicitly track the fluid interface. These features of the diffusion-interface approach enable it to have more potential in the study of multiphase flows where the topological change of the interfaces is complicated. The numerical methods based on diffusion-interface approach can be classified into two kinds: the traditional numerical method based on the phase-field theory (Lowengrub and Truskinovsky, 1978; Hohenberg et al., 1997; Shen, 2012; Kim et al., 2017) and the lattice Boltzmann method (LBM) based on kinetic theory (Aidun and Clausen, 2010; Guo and Shu, 2013; Huang et al., 2015). In the phase-field theory, an order parameter governed by the convection-diffusion type equation [Cahn-Hilliard equation (CHE) (Cahn and Hilliard, 1958; Cahn and Hilliard, 1959) or Allen-Cahn equation (ACE) (Allen and Cahn, 1976)] is used to track the interface. The macroscopic quantities of the fluids (e.g., density and viscosity) are expressed as a function of the order parameter. Up to now, some traditional numerical methods based on phase-field theory, including the finite-difference method (Jacqmin, 1999; Kim et al., 2014; Zhai et al., 2015; Lee and Kim, 2016; Kim et al., 2017), the finite-element method (Zhang and Wang, 2010; Hua et al., 2011), the spectral method (Liu and Shen, 2003; Shen, 2012), and to name but a few, have been successfully adopted to study the multiphase fluid flows (Ding et al., 2007; Yang et al., 2013). However, for some complex multiphase flow, these traditional numerical methods may suffer from the difficulty in treating complex boundaries, the inconvenience in describing the interaction between different phases, the low performance in parallel computing. These shortcomings also limit the

application of these methods in reality (Scarbolo et al., 2013). As an alternative to these traditional numerical methods, the LBM (Guo and Shu, 2013; Krüger et al., 2017) can also be considered as an effective method for complex multiphase flows (Inamuro et al., 2000; Lallemand and Luo, 2000; Liang et al., 2014; Zheng et al., 2015) and nonlinear physical systems (Shi and Guo, 2009; Chai et al., 2016; Chai et al., 2018a).

The LBM for multiphase flows can be commonly classified into four categories: the color-gradient model (Gunstensen et al., 1991), the pseudopotential model (Shan and Chen, 1993; Shan and Chen, 1994), the free-energy model (Swift et al., 1995) and the phase-field-based model (He et al., 1999a). Although these different models have obtain great success in the study of different physical problems (Chen et al., 2014; Liu et al., 2016, Li et al., 2016), here we only focus on the phase-field-based model for its advantages in numerical stability and accuracy for multiphase flow problems with large density and viscosity ratios (Liang et al., 2018). In the phase-field-based model, two lattice Boltzmann (LB) equations are considered, one is used for flow field, and the other is adopted for the phase field. He et al. (1999a) first proposed a phase-field-based LB model (HCZ model) for incompressible multiphase flows. Based on this model, they also investigated two and three-dimensional Rayleigh-Taylor instability problems (He et al., 1999b). Then Lee and Lin (2005) presented a similar LB model where the mixed finite-difference scheme is adopted to improve the stability of HCZ model. However, as point out by Zheng et al. (2005), these two LB models (He et al., 1999a; Lee and Lin, 2005) cannot correctly recover the interface governing equation (CHE) and also contain some assumptions. To give correct macroscopic CHE, they developed a new LB model (Zheng et al., 2005; Zheng et al., 2006) though introducing a spatial difference term of the distribution function. Although the model can recover the CHE, and is also extended to simulate the three-dimensional multiphase flows (Zheng et al., 2008), but the model is limited to the gas-liquid two-phase flow established by Boussinesq approximation (Fakhari et al., 2010). Following a similar idea, Zu and He (2013) adopted a spatial difference term of the equilibrium distribution function such that the CHE can also be recovered correctly. Additionally, based on the LB model for incompressible fluid flows (Guo et al., 2000), they also presented another LB equation for fluid field. In this model, however, the calculations of pressure and velocity are implicit. Different from the previous work (Zheng et al., 2005; Zu and He, 2013), Liang et al. proposed an LB model for CHE in which a time-derivative term is introduced into the evolution function (Liang et al., 2014), and the additional terms appeared in the recovered equations (He et al., 1999a; Lee and Lin, 2005) can be removed. In addition, the calculations of macroscopic pressure and velocity are much easier. Recently, this model is also extended to the three-dimensional case (Liang et al., 2017).

It is known that the CHE can conserve the mass of multiphase system, while the ACE cannot, most of the work based on LB method mainly focused on the CHE (Zheng et al., 2005; Fakhari et al., 2010; Zu and He, 2013; Liang et al., 2014; Yang et al., 2016). However, from the theoretical point

of view, the CHE is a fourth-order partial differential equation, and cannot be recovered from LB model through the second-order Chapman-Enskog expansion (Geier et al., 2015; Wang et al., 2016). On the other hand, from the numerical point of view, the collision process in the LB models for CHE cannot be implemented locally since the nonlocal finite-difference schemes are needed to calculate the spatial derivative of order parameter (Zheng et al., 2005; Fakhari et al., 2010; Zu and He, 2013; Liang et al., 2014). To solve above problems inherent in the LB models for CHE, Geier et al. developed a central-moment LB model for the local ACE (a local gradient term is added to the non-conservative ACE) with mass conservation (Sun and Beckermann, 2007; Chiu et al., 2011), and found the convergence rate of LB model for ACE is higher than that for CHE. Subsequently, Fakhari et al. (2016b) presented a finite-difference LB model for ACE where the Lax-Wendroff scheme is adopted. However, these available LB models cannot recover the ACE correctly. To overcome the drawback, Ren et al. (2016a) and Wang et al. (2016) independently proposed two LB models for ACE, and performed a comparative study of the LB models for ACE and CHE. The results show that the LB model for ACE is more stable. Liang et al. (2018) further presented a simple and accurate LB model for two-phase flows based on the Allen-Cahn phase-field theory, and found that the model is more accurate than the previous LB model (Ren et al., 2016a), especially for the problem with a large density ratio. Recently, Liu et al. (2019) proposed an Allen-Cahn phase-field based LB model for two-phase electro-hydrodynamic flows, and found that the numerical results are in good agreement with some available work. However, we would like to point out that in the aforementioned LB models for local ACE, a term related to the spatial derivative of order parameter is included in the source term (Ren et al., 2016a; Wang et al., 2016; Chai et al., 2018b; Liang et al., 2018) or the equilibrium distribution function (Geier et al., 2015; Fakhari et al., 2016b), and the computation of the term may decrease the accuracy (Wang et al., 2016; Liang et al., 2018) or give rise to some difficulties in implementing the collision process locally (Ren et al., 2016a). On the other hand, another type of conservative ACE named nonlocal ACE is also used to describe phase field, in which a nonlocal integral term is included (Rubinstein and Sternberg, 1992; Brassel and Bretin, 2011; Kim et al., 2014, Lee and Kim, 2016). In the framework of LBM, Chai et al. (2018b) first presented a simple multiple-relaxation-time (MRT) LB model for the nonlocal ACE, and found that through the Chapman-Enskog expansion, the nonlocal ACE can be recovered correctly from the developed LB model. Then they also conducted a comparison between local and nonlocal ACEs, and the numerical results show that both local and nonlocal ACEs can preserve mass conservation of system and each phase, the local ACE is more accurate than nonlocal ACE in capturing the interface profile, but the latter is more stable than the former. Based on these previous results, Hu et al. (2019a) developed an MRT model for a hybrid ACE which is a linear combination of the local and nonlocal ACEs. The results in this work indicate that compared to the local ACE, the hybrid ACE can reduce the numerical dispersion.

The rest of present paper is organized as follows. In Sec.

2, the phase-field models for incompressible multiphase flows are first introduced, then in Sec. 3, some recent progress on the phase-field-based LB models are presented. In addition, some application are discussed in Sec. 4, and finally, we make a summary in Sec. 5.

2. Phase-field models for two-phase flows

We consider a mixture of two immiscible, incompressible Newtonian fluids with densities ρ_A , ρ_B and viscosities μ_A , μ_B . In order to identify the regions occupied by the two fluids, we introduce an order parameter ϕ such that

$$\phi = \frac{\rho - \rho_B}{\rho_A - \rho_B} \phi_A + \frac{\rho - \rho_A}{\rho_B - \rho_A} \phi_B \quad (1)$$

where ϕ_A and ϕ_B are two constants corresponding to ρ_A and ρ_B . For simplicity but without losing generality, the assumption $\phi_A > \phi_B$ is used in the following analysis. The interface of the mixture can be depicted by the set of the order parameter: $\Gamma = \{x : \phi(x, t) = \frac{\phi_A + \phi_B}{2}\}$. In the phase-field theory, the free energy density of a system can be simply written as (Jacqmin, 1999; Lee and Kim, 2012; Shen, 2012)

$$f(\phi, \nabla\phi) = \frac{k}{2} |\nabla\phi|^2 + \psi(\phi) \quad (2)$$

where k is a positive constant, and is also related to the interfacial thickness D and the surface tension σ (see the following discussion). It is clear that the free energy density defined by Eq. (2) includes two parts: the first term is gradient energy, and the second term $\psi(\phi)$ is bulk energy with two minima for a two-phase system. Usually, the bulk energy can be approximated by (Lee and Kim, 2012; Shen, 2012)

$$\psi(\phi) = \beta(\phi - \phi_A)^2(\phi - \phi_B)^2 \quad (3)$$

where β is also a constant relating to the interfacial thickness and the surface tension (see the following discussion). Based on the free energy density mentioned above, one can also define the mixing energy F and chemical potential μ ,

$$\begin{aligned} F(\phi, \nabla\phi) &= \int_{\Omega} f(\phi, \nabla\phi) d\Omega \\ &= \int_{\Omega} [\psi(\phi) + \frac{k}{2} |\nabla\phi|^2] d\Omega \end{aligned} \quad (4)$$

$$\begin{aligned} \mu &= \frac{\delta F}{\delta \phi} \\ &= -\nabla \cdot \left(\frac{\partial F}{\partial \nabla\phi} \right) + \frac{\partial F}{\partial \phi} \\ &= -k\nabla^2\phi + \psi'(\phi) \end{aligned} \quad (5)$$

where Ω is the physical domain occupied by the system, ψ' is the derivative of function ψ with respect to ϕ ,

$$\psi'(\phi) = 4\beta(\phi - \phi_A)(\phi - \phi_B) \left(\phi - \frac{\phi_A + \phi_B}{2} \right) \quad (6)$$

When the diffusive interface is at equilibrium, the chemical potential is zero,

$$\mu = \frac{\delta F}{\delta \phi} = -k\nabla^2\phi + \psi'(\phi) = 0 \quad (7)$$

For one-dimensional problem, one can obtain the interface profile at the equilibrium state by solving Eq. (7) with the relation of $\frac{d\phi}{dx}|_{x \rightarrow \pm\infty} = 0$,

$$\phi(x) = \frac{\phi_A + \phi_B}{2} + \frac{\phi_A - \phi_B}{2} \tanh\left(\sqrt{\frac{2\beta}{k}} \frac{\phi_A - \phi_B}{2}\right)x \quad (8)$$

If we introduce the parameter D to denote the interfacial thickness, Eq. (8) can be rewritten as

$$\phi(x) = \frac{\phi_A + \phi_B}{2} + \frac{\phi_A - \phi_B}{2} \tanh\left(\frac{2x}{D}\right) \quad (9)$$

where D is defined by

$$D = \frac{1}{\phi_A - \phi_B} \sqrt{\frac{8k}{\beta}} \quad (10)$$

Assume that the diffusive mixing energy in the region equals to the traditional surface energy, then the surface tension σ can be written as follows,

$$\sigma = k \int_{-\infty}^{+\infty} \left(\frac{d\phi}{dx} \right)^2 dx \quad (11)$$

After some manipulations, one can obtain

$$\sigma = \frac{(\phi_A - \phi_B)^3}{6} \sqrt{2k\beta} \quad (12)$$

In the phase-field model for multiphase flows, in addition to CHE or ACE for the order parameter, the Navier-Stokes equations for the velocity and pressure are also needed. In the following, we will give a brief introduction to these mathematical equations.

2.1 Cahn-Hilliard equation

If we consider a two phase system advected by the fluid velocity \mathbf{u} and the diffusion is driven by the chemical potential gradient, then the order parameter ϕ can be described by the following CHE,

$$\partial_t \phi + \nabla \cdot (\phi \mathbf{u}) = \nabla \cdot (M_\phi \nabla \mu) \quad (13)$$

where M_ϕ is the mobility coefficient. Note that the CHE can conserve the mass locally, but it is a fourth-order partial differential equation. Therefore, essentially we need a high-order numerical scheme to solve this equation.

2.2 Local Allen-Cahn equation with mass conservation

Based on the previous work (Sun and Beckermann, 2007), the interface advection equation can be written as

$$\phi_t + (u_n \mathbf{n} + \mathbf{u}) \cdot \nabla \phi = 0 \quad (14)$$

where \mathbf{u} is an external advection velocity, \mathbf{n} and u_n are the unit normal vector and normal interface speed, and can be given by

$$\mathbf{n} = \frac{\nabla \phi}{|\nabla \phi|}, \quad u_n = -M_\phi \kappa \quad (15)$$

M_ϕ is a positive constant, and is also named mobility. κ is the interface curvature, and can be expressed as

$$\kappa = \nabla \cdot \mathbf{n} = \nabla \cdot \left(\frac{\nabla \phi}{|\nabla \phi|} \right) = \frac{1}{|\nabla \phi|} \left[\nabla^2 \phi - \frac{(\nabla \phi \cdot \nabla) |\nabla \phi|}{|\nabla \phi|} \right] \quad (16)$$

With the equilibrium distribution defined by Eq.(8), the gradient of ϕ and its normal can be determined by

$$|\nabla \phi| = \frac{d\phi}{dx} = \sqrt{\frac{2\beta}{k}} (\phi_A - \phi)(\phi - \phi_B) = \frac{-4(\phi - \phi_A)(\phi - \phi_B)}{D(\phi_A - \phi_B)} \quad (17)$$

$$\frac{(\nabla \phi \cdot \nabla) |\nabla \phi|}{|\nabla \phi|} = \frac{4\beta}{k} (\phi - \phi_A)(\phi - \phi_B) \left(\phi - \frac{\phi_A + \phi_B}{2} \right) \quad (18)$$

Substituting Eq. (18) into Eq. (16), we can derive the expression of curvature,

$$\kappa = \frac{1}{|\nabla \phi|} \left[\nabla^2 \phi - \frac{4\beta}{k} (\phi - \phi_A)(\phi - \phi_B) \left(\phi - \frac{\phi_A + \phi_B}{2} \right) \right] \quad (19)$$

With the help of Eqs. (15) and (19), one can rewrite Eq. (14) as

$$\phi_t + \mathbf{u} \cdot \nabla \phi = M_\phi \left[\nabla^2 \phi - \frac{4\beta}{k} (\phi - \phi_A)(\phi - \phi_B) \left(\phi - \frac{\phi_A + \phi_B}{2} \right) \right] \quad (20)$$

To describe the case of no curvature-driven interface motion (Sun and Beckermann, 2007; Chiu and Lin, 2011), the counter term approach introduced by Folch et al. (1999) is adopted, and consequently, Eq. (20) can be modified by

$$\begin{aligned} \phi_t + \mathbf{u} \cdot \nabla \phi &= M_\phi \left[\nabla^2 \phi - \frac{4\beta}{k} (\phi - \phi_A)(\phi - \phi_B) \left(\phi - \frac{\phi_A + \phi_B}{2} \right) \right] \\ &\quad - M_\phi \left[|\nabla \phi| \nabla \cdot \left(\frac{\nabla \phi}{|\nabla \phi|} \right) \right] \end{aligned} \quad (21)$$

Then following the procedure in Ref. (Chiu and Lin, 2011) and under the incompressible condition ($\nabla \cdot \mathbf{u} = 0$), Eq. (20) can also be reformulated in a conservative form,

$$\begin{aligned} \phi_t + \nabla \cdot (\phi \mathbf{u}) &= M_\phi \left[\nabla^2 \phi - \nabla \cdot \left(\sqrt{\frac{2\beta}{k}} (\phi_A - \phi)(\phi - \phi_B) \frac{\nabla \phi}{|\nabla \phi|} \right) \right] \\ &= M_\phi \nabla \cdot \left[\left(1 - \sqrt{\frac{2\beta}{k}} (\phi_A - \phi)(\phi - \phi_B) \frac{1}{|\nabla \phi|} \right) \nabla \phi \right] \end{aligned} \quad (22)$$

which is considered as the local ACE, and can also be obtained with the approach shown in Ref. (Geier et al., 2015).

2.2 Nonlocal Allen-Cahn equation with mass conservation

In the phase-field theory, the dynamics of the order parameter ϕ can also be determined by the gradient flow (Shen, 2012),

$$\phi_t + \mathbf{u} \cdot \nabla \phi = -M_\phi \frac{\delta F}{\delta \phi} \quad (23)$$

If we take the variational derivative $\delta F/\delta\phi$ in L^2 space, the following ACE can be obtained,

$$\phi_t + \mathbf{u} \cdot \nabla \phi = M_\phi (\nabla^2 \phi - \psi') \quad (24)$$

Here it should be noted that this classical ACE (Eq. (24)) cannot conserve the mass of system under the appropriate boundary conditions ($\mathbf{n} \cdot \mathbf{u}|_{\partial\Omega} = 0$ and $\mathbf{n} \cdot \nabla \phi = 0$) (Yue et al., 2007), which can be seen clearly through the following equation,

$$\begin{aligned} \frac{d}{dt} \int_{\Omega} \phi d\mathbf{x} + \int_{\Omega} \mathbf{u} \cdot \nabla \phi d\mathbf{x} &= \int_{\Omega} \phi_t d\mathbf{x} + \int_{\partial\Omega} \mathbf{n} \cdot \phi \mathbf{u} ds \\ &= \int_{\Omega} \phi_t d\mathbf{x} = M_\phi \int_{\Omega} (\nabla^2 \phi - \psi') d\mathbf{x} \\ &= M_\phi \int_{\partial\Omega} \mathbf{n} \cdot \nabla \phi ds - M_\phi \int_{\Omega} \psi' d\mathbf{x} \\ &= -M_\phi \int_{\Omega} \psi' d\mathbf{x} \end{aligned} \quad (25)$$

From the Eq. (25), we can find that the term $\int_{\Omega} \psi' d\mathbf{x}$ is not always zero, and the ACE cannot conserve the mass. To overcome this problem, Rubinstein and Sternberg (1992) introduce a nonlocal Lagrange multiplier $\beta(t)$ into the ACE,

$$\phi_t + \mathbf{u} \cdot \nabla \phi = M_\phi [\nabla^2 \phi - \psi' + \beta(t) \sqrt{2\psi}] \quad (26)$$

and $\beta(t)$ is defined as

$$\beta(t) = \frac{\int_{\Omega} \psi' d\mathbf{x}}{\int_{\Omega} d\mathbf{x}} \quad (27)$$

Based on above definition of $\beta(t)$, Eq. (26) can satisfy the condition of mass conservation, i.e.,

$$\frac{d}{dt} \int_{\Omega} \phi d\mathbf{x} = 0 \quad (28)$$

We noted that Eq. (26) is also called the nonlocal ACE (Chai et al., 2018b).

2.4 Navier-Stokes equations

For two-phase flows, the Navier-Stokes equations (NSEs) are used to describe the flow field. For simplicity, here we only focus on the following NSEs for incompressible fluid flows (Jacqmin, 1999; Kendon et al., 2001; Bandalassi et al., 2003)

$$\nabla \cdot \mathbf{u} = 0 \quad (29)$$

$$\rho \left(\frac{\partial \mathbf{u}}{\partial t} + \mathbf{u} \cdot \nabla \mathbf{u} \right) = -\nabla p + \nabla \cdot [\rho v(\nabla \mathbf{u} + \nabla \mathbf{u}^T)] + \mathbf{F}_s + \mathbf{G} \quad (30)$$

where \mathbf{u} denotes the fluid velocity, p is the hydrodynamic pressure, v represents the kinematic viscosity. \mathbf{G} is the body force, \mathbf{F}_s is the interfacial force, and is given by (Liu, et al., 2014)

$$\mathbf{F}_s = (-\sigma \mathbf{k} \mathbf{n} + \nabla_s \sigma) \delta \quad (31)$$

where σ denotes surface tension, $\nabla_s = (\mathbf{I} - \mathbf{n}\mathbf{n}) \cdot \nabla$ is the surface gradient operator, and δ accounts for the Dirac delta function, which can be expressed as $\delta = \alpha |\nabla \phi|^2$ and satisfy

$$\int_{-\infty}^{+\infty} \delta dx = 1$$

After some algebraic manipulations, one can obtain

$$\alpha \int_{-\infty}^{+\infty} \frac{2\beta}{k} (\phi - \phi_A)^2 (\phi - \phi_B)^2 dx = 1 \quad (32)$$

$$\alpha = \frac{6\sqrt{k}}{\sqrt{2\beta}(\phi_A - \phi_B)^3} \quad (33)$$

With the aid of Eq. (33), Eq. (31) can be rewritten as

$$\mathbf{F}_s = \frac{6\sqrt{k}}{\sqrt{2\beta}(\phi_A - \phi_B)^3} \nabla \cdot [\sigma |\nabla \phi|^2 \mathbf{I} - \sigma \nabla \phi \nabla \phi] \quad (34)$$

Actually, the interfacial force [Eq. (34)] can be transformed into a equivalent potential form (Liu, et al., 2014),

$$\mathbf{F}_s = \frac{6\sqrt{k}}{\sqrt{2\beta}(\phi_A - \phi_B)^3} [|\nabla \phi|^2 \nabla \sigma - \nabla \sigma \cdot (\nabla \phi \nabla \phi) + \frac{\sigma}{k} \mu \nabla \phi] \quad (35)$$

In particular, if the interfacial tension is a constant, the interfacial force term would reduce to the following form,

$$\mathbf{F}_s = \frac{\alpha \sigma}{k} \mu \nabla \phi = \mu \nabla \phi \quad (36)$$

3. Phase-field-based LB models for incompressible multiphase flows

In the past decades, the LBM, as a mesoscopic numerical approach, has gained a great success in the study of complex fluid flows and physical systems governed by some particular partial differential equations (Succi, 2001; Guo and Shu, 2013; Chai et al., 2016; Kürger, 2017; Chai et al., 2019). The general evolution equation of the LBM can be written as

$$\begin{aligned} h_i(\mathbf{x} + \mathbf{c}_i \Delta t, t + \Delta t) - h_i(\mathbf{x}, t) \\ = -\Lambda_{ij}^h [h_j(\mathbf{x}, t) - h_j^{eq}(\mathbf{x}, t)] + \Delta t R_i(\mathbf{x}, t) \end{aligned} \quad (37)$$

where $h_i(\mathbf{x}, t)$ ($h = f$ for phase field and $h = g$ for flow field) is the distribution function with velocity \mathbf{c}_i at position \mathbf{x} and time t , Λ_{ij}^h is an element of the generalized collision matrix Λ^h , and $R_i(\mathbf{x}, t)$ is the source or force term. $h_i^{eq}(\mathbf{x}, t)$ is the

local equilibrium distribution function, which is related to the macroscopic quantities, discrete velocity \mathbf{c}_i , the speed of sound c_s , and the weight coefficient w_i . In the commonly used D2Q9 (nine velocities in two-dimensional space) lattice model, the discrete velocity \mathbf{c}_i , the speed of sound c_s , and the weight coefficient w_i can be defined by

$$\mathbf{c}_i = c \begin{bmatrix} 0 & 1 & 0 & -1 & 0 & 1 & -1 & -1 & 1 \\ 0 & 0 & 1 & 0 & -1 & 1 & 1 & -1 & -1 \end{bmatrix}$$

$$w_i = \begin{cases} \frac{4}{9}, & i=0 \\ \frac{1}{9}, & i=1, \dots, 4 \\ \frac{1}{36}, & i=5, \dots, 8 \end{cases}, \quad c_s^2 = c^2/3 \quad (38)$$

For the collision matrix Λ^h , there are two basic kinds, i.e., the single-relaxation-time (SRT) and the MRT models (d'Humerie, 1992; Qian et al., 1992). In the SRT model, the collision matrix is given by $\Lambda^h = \mathbf{I}/\tau_h$ with \mathbf{I} representing the unit matrix, while in the MRT model, Λ^h be written as (Lallemand et al., 2000),

$$\Lambda^h = \mathbf{M}^{-1} \mathbf{S}^h \mathbf{M} \quad (39)$$

where \mathbf{M} is the transformation matrix, and in the D2Q9 lattice model, \mathbf{M} is given as

$$\mathbf{M} = \begin{pmatrix} 1 & 1 & 1 & 1 & 1 & 1 & 1 & 1 & 1 \\ -4 & -1 & -1 & -1 & -1 & 2 & 2 & 2 & 2 \\ 4 & -2 & -2 & -2 & -2 & 1 & 1 & 1 & 1 \\ 0 & 1 & 0 & -1 & 0 & 1 & -1 & -1 & 1 \\ 0 & -2 & 0 & 2 & 0 & 1 & -1 & -1 & 1 \\ 0 & 0 & 1 & 0 & -1 & 1 & 1 & -1 & -1 \\ 0 & 0 & -2 & 0 & 2 & 1 & 1 & -1 & -1 \\ 0 & 1 & -1 & 1 & -1 & 0 & 0 & 0 & 0 \\ 0 & 0 & 0 & 0 & 0 & 1 & -1 & 1 & -1 \end{pmatrix}$$

which can be used to project h_i and h_i^{eq} onto the moment space with $\mathbf{m}_h = \mathbf{M}\mathbf{h}$ and $\mathbf{m}_h^{eq} = \mathbf{M}\mathbf{h}^{eq}$, where $\mathbf{h} = (h_0, \dots, h_8)^T$ and $\mathbf{h}^{eq} = (h_0^{eq}, \dots, h_8^{eq})^T$. \mathbf{S}^h is a diagonal relaxation matrix,

$$\mathbf{S}^h = diag(s_0^h, s_1^h, s_2^h, s_3^h, s_4^h, s_5^h, s_6^h, s_7^h, s_8^h) \quad (40)$$

where $0 < s_i^h < 2$.

3.1 The LB model for Cahn-Hilliard equation

For the phase-field-based LB model, He et al. (1999a) first adopted the index function to track the interface. Nevertheless, Zheng et al. (2005, 2006) point out that the model (He et al., 1999a) cannot be completely recovered to CHE, then they (Zheng et al., 2005) presented a new LB model for interface capturing in which a spatial difference term of the distribution function was introduced. In the model of Zheng et al., the source term in the Eq. (37) can be expressed as

$$R_i = \frac{(1-q)[f_i(\mathbf{x} + \mathbf{c}_i \Delta t, t) - f_i(\mathbf{x}, t)]}{\Delta t} \quad (41)$$

where the parameter q is a constant, and is given by

$$q = \frac{1}{\tau_f + 0.5} \quad (42)$$

where $\tau_f = 1/s_3^f = 1/s_5^f$. The local equilibrium distribution function is defined as

$$f_i^{eq}(\mathbf{x}, t) = \begin{cases} \phi - 2\eta\mu, & i=0 \\ \frac{1}{2}\eta\mu + \frac{1}{2q}\mathbf{c}_i \cdot \phi\mathbf{u}, & i \neq 0 \end{cases}$$

where η is an adjustable parameter that controls the mobility M_ϕ ,

$$M_\phi = \eta q (\tau_f q - 0.5) \Delta t \quad (43)$$

The order parameter is calculated by

$$\phi = \sum_i f_i \quad (44)$$

Following the similar idea, Zu and He (2013) developed another LB model where a spatial difference term of the equilibrium distribution function instead of the distribution function is adopted. In the model of Zu and He (2013), the source term and local equilibrium distribution function are given by

$$R_i = \frac{(2\tau_f - 1)[f_i^{eq}(\mathbf{x} + \mathbf{c}_i \Delta t, t) - f_i^{eq}(\mathbf{x}, t)]}{\Delta t} \quad (45)$$

$$f_i^{eq}(\mathbf{x}, t) = \begin{cases} \phi - \frac{(1-w_0)\eta\mu}{2(1-\tau_f)c_s^2}, & i=0 \\ w_i \frac{\eta\mu + \mathbf{c}_i \cdot \phi\mathbf{u}}{2(1-\tau_f)c_s^2}, & i \neq 0 \end{cases}$$

In addition, the mobility M_ϕ is related to the relaxation time τ_f ,

$$M_\phi = \eta(\tau_f - 0.5) \Delta t \quad (46)$$

The macroscopic order parameter is still evaluated by Eq. (44). Here it should be noted that in the model of Zu and He (2013), the term of $1/(\tau_f - 1)$ included in the equilibrium distribution would cause instability problem as the relaxation time approaches 1.

Recently, Liang et al. (2014) presented an MRT model for CHE in which a time-derivative term is introduced into the evolution function (Chopard et al., 2009), and the macroscopic CHE can be recovered correctly from the LB model. In the model of Liang et al. (2014), the source term R_i in Eq. (37) is expressed as (Guo et al., 2008; Chai and Zhao, 2012)

$$\mathbf{R} = \mathbf{M}^{-1} \left(\mathbf{I} - \frac{\mathbf{S}^f}{2} \right) \mathbf{M} \bar{\mathbf{R}} \quad (47)$$

where $\mathbf{R} = (R_0, \dots, R_8)$, $\bar{\mathbf{R}} = (\bar{R}_0, \dots, \bar{R}_8)$ with

$$\bar{R}_i = \frac{w_i \mathbf{c}_i \cdot \partial_t(\phi\mathbf{u})}{c_s^2} \quad (48)$$

Here we need to use the finite-difference method to compute the time derivative term $\partial_t \phi \mathbf{u}$, for simplicity, the following explicit finite-difference scheme is adopted (Shi et al., 2008),

$$\partial_t(\phi \mathbf{u})(\mathbf{x}, t) = [(\phi \mathbf{u})(\mathbf{x}, t) - (\phi \mathbf{u})(\mathbf{x}, t - \Delta t)] / \Delta t \quad (49)$$

The local equilibrium distribution in the model of Liang et al. (2014) is given by

$$f_i^{eq}(\mathbf{x}, t) = \begin{cases} \phi + (w_i - 1)\eta\mu, & i = 0 \\ w_i\eta\mu + w_i \frac{\mathbf{c}_i \cdot (\phi \mathbf{u})}{c_s^2}, & i \neq 0 \end{cases}$$

where the parameter η can be used to adjust the mobility M_ϕ ,

$$M_\phi = \eta c_s^2 (\tau_f - 0.5) \Delta t \quad (50)$$

Here the order parameter can be still calculated by Eq. (44). We would like to point out that the chemical potential appeared in the equilibrium distribution function includes a second-order spatial derivative of order parameter, and the second-order isotropic central schemes are adopted to preserve the global mass conservation (Guo et al., 2011; Lou et al., 2012),

$$\nabla \chi(\mathbf{x}, t) = \sum_{i \neq 0} \frac{w_i \mathbf{c}_i \chi(\mathbf{x} + \mathbf{c}_i \Delta t, t)}{c_s^2 \Delta t} \quad (51a)$$

$$\nabla^2 \chi(\mathbf{x}, t) = \sum_{i \neq 0} \frac{2w_i \mathbf{c}_i [\chi(\mathbf{x} + \mathbf{c}_i \Delta t, t) - \chi(\mathbf{x}, t)]}{c_s^2 \Delta t^2} \quad (51b)$$

where χ is an arbitrary function.

3.2 The LB model for the local Allen-Cahn equation

However, from the theoretical point of view, the CHE is a fourth-order partial differential equation, and through the Chapman-Enskog analysis, it cannot be directly recovered from the LB models (Wang et al., 2016). On the other hand, from the numerical point of view, the most appealing property, i.e., locality of collision process, cannot be preserved in the LB models for CHE since the nonlocal finite-difference schemes are needed to calculate space derivatives of order parameter (Zheng et al., 2005, 2006; Zu and He, 2013; Liang et al., 2014, 2016b). To solve above problems, the LB models for second-order ACE are desirable.

Geier et al. (2015) first developed a central-moment LB model for local ACE. In the model of Geier et al. (2015), the source term in the Eq. (37) is set to be zero, and the local equilibrium distribution function is defined as

$$f_i^{eq}(\mathbf{x}, t) = \phi w_i \left(1 + \frac{\mathbf{c}_i \cdot \mathbf{u}}{c_s^2} + \frac{(\mathbf{c}_i \cdot \mathbf{u})^2}{2c_s^4} - \frac{\mathbf{u}_i \cdot \mathbf{u}}{2c_s^2} \right) + \frac{M_\phi \theta}{c_s^2} w_i \mathbf{c}_i \cdot \mathbf{n} \quad (52)$$

where $\theta = \sqrt{\frac{2\beta}{k}} (\phi_A - \phi)(\phi - \phi_B)$, $\mathbf{n} = \frac{\nabla \phi}{|\nabla \phi|}$, and the mobility M_ϕ is given by

$$M_\phi = c_s^2 (\tau_f - 0.5) \Delta t \quad (53)$$

The order parameter is computed by

$$\phi = \sum_i f_i \quad (54)$$

However, as pointed out by Ren et al. (2016a), the LB model of Geier et al. (2015) cannot give the correct local ACE. To overcome the problem, they proposed an improved MRT model for the same ACE. In their model, the source term in Eq. (37) can be given by

$$\mathbf{R} = \mathbf{M}^{-1} \left(\mathbf{I} - \frac{\mathbf{S}^f}{2} \right) \mathbf{M} \bar{\mathbf{R}} \quad (55)$$

where $\mathbf{R} = (R_0, \dots, R_8)$, $\bar{\mathbf{R}} = (\bar{R}_0, \dots, \bar{R}_8)$ with

$$\bar{R}_i = \frac{w_i \mathbf{c}_i \cdot (\partial_t(\phi \mathbf{u}) + \theta \mathbf{n})}{c_s^2} \quad (56)$$

It should be noted that the time and space derivative terms in above equation are computed through Eqs. (49) and (51a). In the model of Ren et al (2016a), the local equilibrium distribution is defined as

$$f_i^{eq}(\mathbf{x}, t) = \phi w_i \left(1 + \frac{\mathbf{c}_i \cdot \mathbf{u}}{c_s^2} \right) \quad (57)$$

In addition, the mobility M_ϕ is given by Eq. (53), and the order parameter can also be calculated by Eq. (54). We noted that almost at the same time, Wang et al. (2016) also independently developed a new LB model for local ACE, which can be viewed as a SRT version of the model of Ren et al. (2016a). In their model, however, the gradient of the order parameter is computed locally through first-order moments of the non-equilibrium distribution function.

3.3 The LB model for the nonlocal Allen-Cahn equation

In the framework of LBM, Chai et al. (2018b) first developed an MRT model for the nonlocal ACE where the advection is neglected. Actually, for nonlocal ACE (Eq. (26)), the source term \mathbf{R} reads

$$\mathbf{R} = \mathbf{M}^{-1} \left(\mathbf{I} - \frac{\mathbf{S}^f}{2} \right) \mathbf{M} \bar{\mathbf{R}} \quad (58)$$

where $\mathbf{R} = (R_1, \dots, R_4)$, $\bar{\mathbf{R}} = (\bar{R}_1, \dots, \bar{R}_4)$ with

$$\bar{R}_i = w_i \left\{ M_\phi \left[-\psi' + \beta(t) \sqrt{2\psi} \right] + \frac{\mathbf{c}_i \cdot \partial_t(\phi \mathbf{u})}{c_s^2} \right\} \quad (59)$$

The local equilibrium distribution is defined as

$$f_i^{eq}(\mathbf{x}, t) = w_i \phi \left[1 + \frac{\mathbf{c}_i \cdot (\phi \mathbf{u})}{c_s^2} \right] \quad (60)$$

and the mobility M_ϕ given by

$$M_\phi = c_s^2 (\tau_f - 0.5) \Delta t \quad (61)$$

where $\tau_f = 1/s_1^f$. Unlike the aforementioned models, the order parameter in this model is calculated as

$$\phi = \sum_i f_i + \frac{\Delta t}{2} \sum_i \bar{R}_i \quad (62)$$

3.4 The LB model for the incompressible Navier-Stokes equations

In addition to the phase field, we need another LB equation for flow field. He et al. (1999a) first proposed an LB scheme for the incompressible multiphase flows. In this LB model, the equilibrium distribution function g_i^{eq} and the force term R_i for the flow field can be written as

$$g_i^{eq} = w_i \left[p + \rho \left(\frac{\mathbf{c}_i \cdot \mathbf{u}}{c_s^2} + \frac{(\mathbf{c}_i \cdot \mathbf{u})^2}{2c_s^4} - \frac{\mathbf{u} \cdot \mathbf{u}}{2c_s^2} \right) \right] \quad (63)$$

$$\begin{aligned} R_i = & \left(1 - \frac{1}{2\tau_g} \right) (\mathbf{c}_i - \mathbf{u}) \cdot [\Gamma_i(\mathbf{u})(\mathbf{F}_s + \mathbf{G}) \\ & - (\Gamma_i(\mathbf{u}) - \Gamma_i(0)) \nabla \Psi(\rho)] \end{aligned} \quad (64)$$

where

$$\Gamma_i(\mathbf{u}) = w_i \left[1 + \frac{\mathbf{c}_i \cdot \mathbf{u}}{c_s^2} + \frac{(\mathbf{c}_i \cdot \mathbf{u})^2}{2c_s^4} - \frac{\mathbf{u} \cdot \mathbf{u}}{2c_s^2} \right] \quad (65)$$

and $\Psi(\rho) = p - \rho c_s^2$. The macroscopic variables can be calculated by

$$p = \sum g_i + \frac{\Delta t}{2} c_s^2 \mathbf{u} \cdot \nabla \rho \quad (66)$$

$$c_s^2 \rho \mathbf{u} = \sum \mathbf{c}_i g_i + \frac{c_s^2 \Delta t}{2} (\mathbf{F}_s + \mathbf{G}) \quad (67)$$

In this model, the kinetic viscosity is related to the relaxation parameter by $\nu = c_s^2 (\tau_g - \frac{1}{2}) \Delta t$ with $\tau_g = 1/s_7^g = 1/s_8^g$ denoting the dimensional relaxation time for the flow field.

Lee and Lin (2005) proposed a stable discretization scheme to calculate the force terms so that a large density ratio can be reached, and considered the following surface tension in the NSEs,

$$\mathbf{F}_s = k \nabla \cdot [(\nabla \rho) \cdot (\nabla \rho) \mathbf{I} - (\nabla \rho) \otimes (\nabla \rho)] \quad (68)$$

The equilibrium distribution function, the force term R_i , and the computation of the macroscopic variables are the same as those in the LB model of He et al. (1999a). Base on the models of He et al. (1999a) and Lee and Lin (2005), some improved LB models for the multiphase flows are also developed (Li et al., 2012; Fakhari and Rahimian, 2016a; Yang et al., 2016; Zheng et al., 2019).

Different from the models mentioned above, Zheng et al. (2006) developed a new LB model for multiphase flows, and claimed that his model could deal with two-phase flows with large density ratios. While Fakhari et al. (2016a) found that the model can only be used to deal with density-matched binary fluids where the Boussinesq approximation holds. In the model of Zheng et al. (2006) the compressible NSEs are adopted to replace incompressible NSEs where the density ρ is defined as $\rho = \frac{\rho_A + \rho_B}{2}$ with ρ_A and ρ_B being the densities of fluid A and fluid B. The equilibrium distribution function in their is defined as

$$g_i^{eq} = w_i \left[A_i + \rho \left(\frac{\mathbf{c}_i \cdot \mathbf{u}}{c_s^2} + \frac{(\mathbf{c}_i \cdot \mathbf{u})^2}{2c_s^4} - \frac{\mathbf{u} \cdot \mathbf{u}}{2c_s^2} \right) \right] \quad (69)$$

where the coefficients are taken as $A_1 = \frac{9}{4}\rho - \frac{15}{4}(\phi\mu + \frac{1}{3}\rho)$, $A_i|_{i=2,\dots,9} = 3(\phi\mu + \frac{1}{3}\rho)$.

In addition, the force distribution function is given by

$$R_i = \left(1 - \frac{1}{2\tau_g} \right) \frac{w_i}{c_s^2} \left[(\mathbf{c}_i - \mathbf{u}) + \frac{\mathbf{c}_i \cdot \mathbf{u}}{c_s^2} \mathbf{c}_i \right] \cdot (\mu \nabla \phi + \mathbf{G}) \quad (70)$$

and the macroscopic variables are calculated by

$$\rho = \sum g_i \quad (71)$$

$$\rho \mathbf{u} = \sum \mathbf{c}_i g_i + \frac{1}{2} (\mu \nabla \phi + \mathbf{G}) \quad (72)$$

Based on the phase-field theory, Zu and He (2013) proposed an LB model which is capable of dealing with binary fluids with moderate density ratios. However, in their model, a prediction-correction step is needed to calculate the velocity and pressure since they satisfy two implicit equations. Besides, the equilibrium distribution function of the LB model for the NSEs reads

$$g_i^{eq}(\mathbf{x}, t) = \begin{cases} \frac{p}{c_s^2} (w_0 - 1) - w_0 \rho \frac{\mathbf{u} \cdot \mathbf{u}}{c_s^2}, & i = 0, \\ w_i \left[\frac{p}{c_s^2} + \frac{\mathbf{c}_i \cdot \mathbf{u}}{c_s^2} + \frac{(\mathbf{c}_i \cdot \mathbf{u})^2}{2c_s^4} - \frac{\mathbf{u} \cdot \mathbf{u}}{2c_s^2} \right], & i = 1, \dots, q-1 \end{cases} \quad (73)$$

To recover the macroscopic momentum equation correctly, the distribution function for total force should be given by

$$R_i = w_i (\mathbf{c}_i / c_s^2) \cdot \mathbf{F} / \rho \quad (74)$$

where $\mathbf{F} = \mathbf{F}_s + \mathbf{F}_p + \mathbf{F}_\mu + \mathbf{G}$ with $\mathbf{F}_s = -\phi \nabla \mu$, $\mathbf{F}_p = -p \nabla \rho$ and $\mathbf{F}_\mu = [(\tau_g - 1/2)c_s^2 \Delta t](\nabla \mathbf{u} + \mathbf{u} \nabla) \cdot \nabla \rho$.

The macroscopic variables can be evaluated as

$$\mathbf{u} = \sum \mathbf{c}_i g_i + \frac{\mathbf{F}}{2\rho} \Delta t \quad (75)$$

$$p = \left(\sum_{i \neq 0} c_s^2 g_i - w_0 |\mathbf{u}|^2 / 2 \right) / (1 - w_0) \quad (76)$$

To obtain the coupled velocity and pressure, the following prediction-correction technology is adopted,

$$\hat{p} = \left(\sum_{i \neq 0} c_s^2 g_i - w_0 |\mathbf{u}^{t-\Delta t}|^2 / 2 \right) / (1 - w_0) \quad (77a)$$

$$\hat{\mathbf{u}} = \sum \mathbf{c}_i g_i + \frac{\Delta t}{2} [\mathbf{F}_s + \mathbf{F}_p(\hat{p}) + \mathbf{F}_\mu(\mathbf{u}^{t-\Delta t}) + \mathbf{G}] / \rho \quad (77b)$$

$$p = \left(\sum_{i \neq 0} c_s^2 g_i - w_0 |\hat{\mathbf{u}}|^2 / 2 \right) / (1 - w_0) \quad (78a)$$

$$\mathbf{u} = \sum \mathbf{c}_i g_i + \frac{\Delta t}{2} [\mathbf{F}_s + \mathbf{F}_p(p) + \mathbf{F}_\mu(\hat{\mathbf{u}}) + \mathbf{G}] / \rho \quad (78b)$$

Liang et al. (2014) proposed a phase-field-based MRT model for incompressible multiphase flow systems. In their

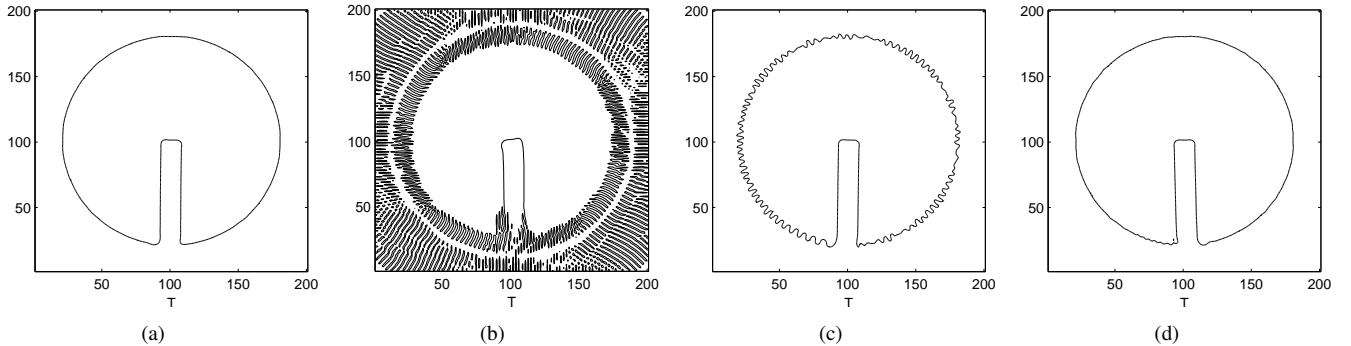


Fig. 1. The comparisons of several phase-field LB models for simulating the Zalesak's disk problem at one period. (a) the phase-field LB model of Liang et al. (2014), (b) the mode of Zheng et al. (2005), (c) the model of Fakhari and Rahimian (2010), (d) the model of Zu and He (2013).

model, the equilibrium distribution function is carefully designed to recover the correct macroscopic NSEs, and is given by

$$g_i^{eq}(\mathbf{x}, t) = \begin{cases} \frac{p}{c_s^2}(w_0 - 1) - w_i \rho \frac{\mathbf{u}^2}{c_s^2}, & i = 0, \\ \frac{p}{c_s^2} w_i + w_i \rho \left[\frac{\mathbf{c}_i \cdot \mathbf{u}}{c_s^2} + \frac{(\mathbf{c}_i \cdot \mathbf{u})^2}{2c_s^4} - \frac{\mathbf{u} \cdot \mathbf{u}}{2c_s^2} \right], & i \neq 0 \end{cases} \quad (79)$$

The force term R_i is defined as

$$R_i = \frac{w_i(\mathbf{c}_i - \mathbf{u})}{2c_s^2} \cdot [(\Gamma_i(\mathbf{u}) - 1)(\nabla(\rho c_s^2) + \Gamma_i(\mathbf{u})(\mathbf{F}_s + \mathbf{F}_a + \mathbf{G})] \quad (80)$$

where $\mathbf{F}_a = \frac{\rho_A - \rho_B}{\phi_A - \phi_B} \nabla \cdot (M_\phi \nabla \mu) \mathbf{u}$ is an interfacial force introduced by Li et al. (2012). In addition, the macroscopic variables are calculated explicitly as

$$\mathbf{u} = \frac{\sum \mathbf{c}_i g_i + 0.5\Delta t (\mathbf{F}_s + \mathbf{G})}{\rho - 0.5\Delta t \frac{\rho_A - \rho_B}{\phi_A - \phi_B} \nabla \cdot (M_\phi \nabla \mu)} \quad (81a)$$

$$p = \frac{c_s^2}{1 - w_0} \left[\sum_{i \neq 0} g_i + 0.5\Delta t \mathbf{u} \cdot \nabla \rho - \rho \frac{\mathbf{u} \cdot \mathbf{u}}{c_s^2} \right] \quad (81b)$$

In a recent work, Liang et al. (2016a) further presented some modifications on the force distribution function and the computation of the macroscopic variables,

$$R_i = w_i \frac{\mathbf{c}_i \cdot \mathbf{F}_a}{c_s^2} + w_i \left(1 - \frac{1}{2\tau_g} \right) \left[\mathbf{u} \cdot \nabla \rho + \frac{\mathbf{c}_i \cdot (\mathbf{F}_s + \mathbf{G})}{c_s^2} \right] + w_i \left(1 - \frac{1}{2\tau_g} \right) \left[\frac{(\mathbf{u}\mathbf{F} + \mathbf{F}\mathbf{u} + \mathbf{u}\nabla c_s^2 \rho + \nabla c_s^2 \rho \mathbf{u}) : Q_i}{2c_s^4} \right] \quad (82)$$

$$\mathbf{u} = \frac{1}{\rho} [\sum \mathbf{c}_i g_i + 0.5\Delta t (\mathbf{F}_s + \mathbf{G})] \quad (83a)$$

$$p = \frac{c_s^2}{1 - w_0} \left[\sum_{i \neq 0} g_i + 0.5\Delta t \mathbf{u} \cdot \nabla \rho - \rho \frac{\mathbf{u} \cdot \mathbf{u}}{c_s^2} \right] \quad (83b)$$

where $Q_i = \mathbf{c}_i \mathbf{c}_i - c_s^2 \mathbf{I}$, $\mathbf{F}_a = \mathbf{u}(\partial_t \rho + \nabla \cdot (\rho \mathbf{u}))$.

4. Applications

In this section, we will present some applications of the phase-field-based LBM for multiphase flow problems, which include the interface-tracking problem, the bubble rising problem, the classic Rayleigh-Taylor instability, and the droplet impact dynamics.

4.1 The interface-tracking problems

Zalesak's disk is a classic benchmark problem to test the capacity of a numerical method in interface capturing. The description of this problem can be given as follows. The disk with a slot is initially placed at the center of a square domain, and a vortex flow with a linear distribution of the velocity field is imposed, which drives the rotation of the disk,

$$u = -w(y - 0.5d), \quad v = w(x - 0.5d) \quad (84)$$

where d is the width of the domain, $w = U_0 \pi / d$ is a constant angular velocity, and the disk will complete one full rotation at the period of $T = 2d/U_0$. We have used an improved Cahn-Hilliard phase-field-based LB model (Liang et al., 2014) to simulate the rotation of the Zalesak's disk, and compared the model with the previous phase-field-based LB models (Zheng et al., 2005; Fakhari and Rahimian, 2010; Zu and He, 2013). The interface patterns of the slotted disk after one period are plotted in Fig. 1. From this figure, it can be seen that the improved model is able to capture an accurate and stable interface of the disk, and some undesirable diffusions around the interface edge or quantities of jetsam can be produced by the previous models. In addition, the model is also used to simulate the challenging interface-capturing problems of time-reversed single vortex and deformation field, in which a large interfacial topological change is induced. In the former example, a circular disk is initially placed in the upper portion of the domain and a strongly nonlinear velocity field is applied,

$$u = U_0 \sin^2 \frac{\pi x}{d} \sin \frac{2\pi y}{d} \cos \frac{\pi t}{T} \quad (85)$$

$$v = -U_0 \sin \frac{2\pi x}{d} \sin^2 \frac{\pi y}{d} \cos \frac{\pi t}{T}$$

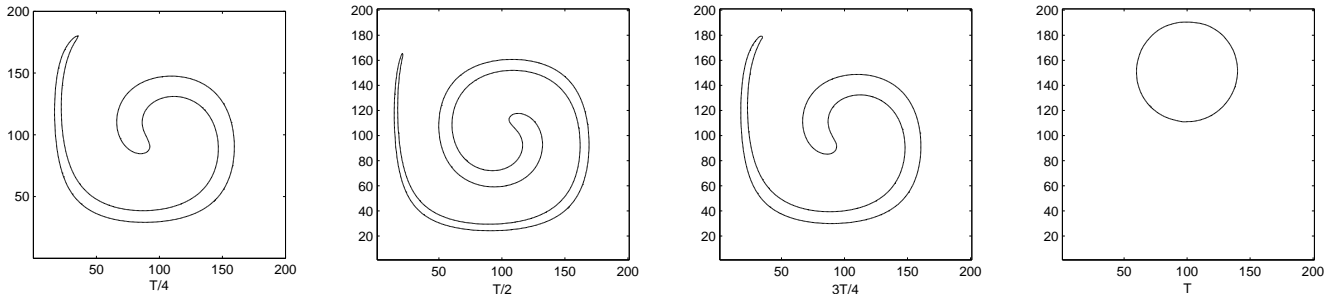


Fig. 2. Simulation of the single vortex by the phase-field LB model of Liang et al. (2014).

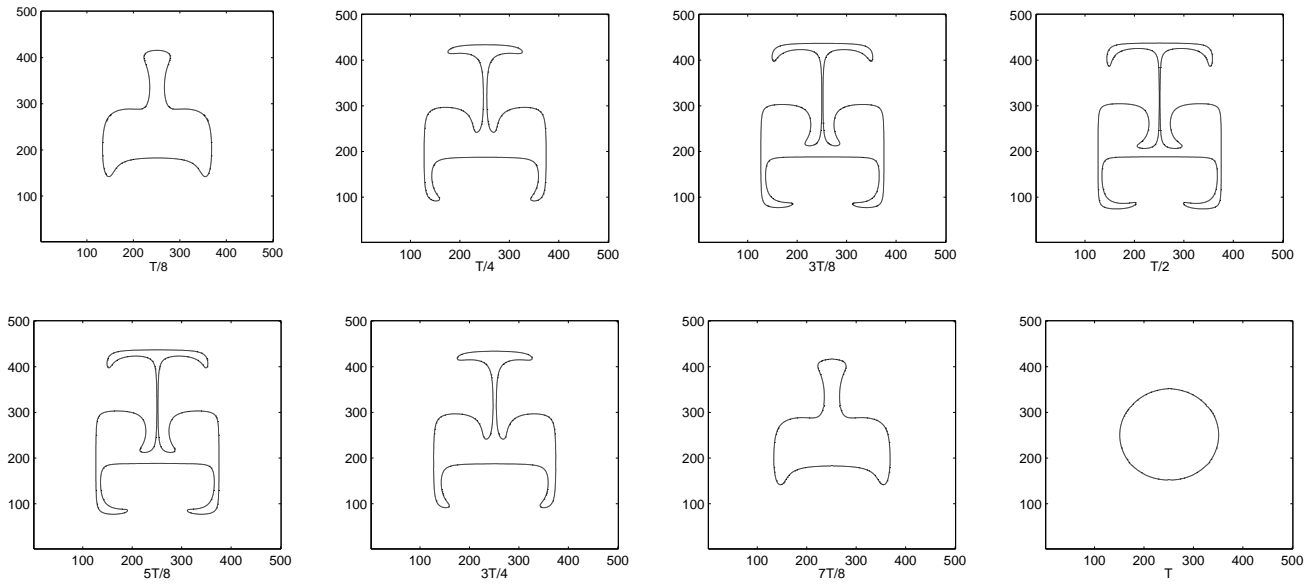


Fig. 3. Simulation of the deformation field by the phase-field LB model of Liang et al. (2014).

where t is dimensionless time scaled by d/U_0 . Theoretically, the disk's interface will be stretched into a thin filament progressively that spirals towards the vortex center until undergoing the largest deformation at time $T/2$. Then, if the velocity field is reversed in time, the disk will return to its initial position at time T . The computational result presented in Fig. 2 shows a good agreement with the theoretical prediction. In the latter test of deformation field, a circular body is initially located in the middle of the domain and a complex velocity distribution is given by

$$u = -U_0 \sin(n\pi(\frac{x}{d} + 0.5)) \sin(n\pi(\frac{y}{d} + 0.5)) \cos \frac{\pi t}{T}$$

$$v = -U_0 \cos(n\pi(\frac{x}{d} + 0.5)) \cos(n\pi(\frac{y}{d} + 0.5)) \cos \frac{\pi t}{T}$$

Fig. 3 shows the evolution of the phase interface in one period T . It is shown that the circular body is continuously entrained by the vortices and a very thin filamentary structure is generated at half period, and then it moves back and returns to the initial configuration at one period. Recently, several types of the LB models (Geier et al., 2015, Ren et al., 2016a, Wang et al., 2016) based on the Allen-Cahn phase

field theory have also been proposed and used to simulate these interface-tracking problems. In general, these LB models can also achieve the satisfactory results in interface capturing.

4.2 The bubble rising problem

The buoyancy-driven motion of bubble is a fundamental two-phase flow problem. The study of such flow dynamics is still important not only in its own unique fluid mechanics, but also in many applications, such as petroleum refining, gas-liquid column reactors and heterogeneous catalysis. Due to its importance, it attracts the attentions of many scientists and also several researchers have used the phase-field-based LB models to investigate the bubble dynamics. For instance, Kurtoglu and Lin (2006) used a modified phase-field-based LB model to simulate two-dimensional single bubble dynamics with a small density ratio of 2.54. Starting from the Cahn-Hilliard theory, Amaya-Bower and Lee (2010) adopted an improved phase-field-based LB model to study the dynamic behavior of single bubble rising with a high density ratio of 1000. Huang et al. (2014) proposed a mass-conserving Cahn-Hilliard-based LB model in the axisymmetric coordinate system and applied it to simulate single bubble rising with a density ratio of 15.5.

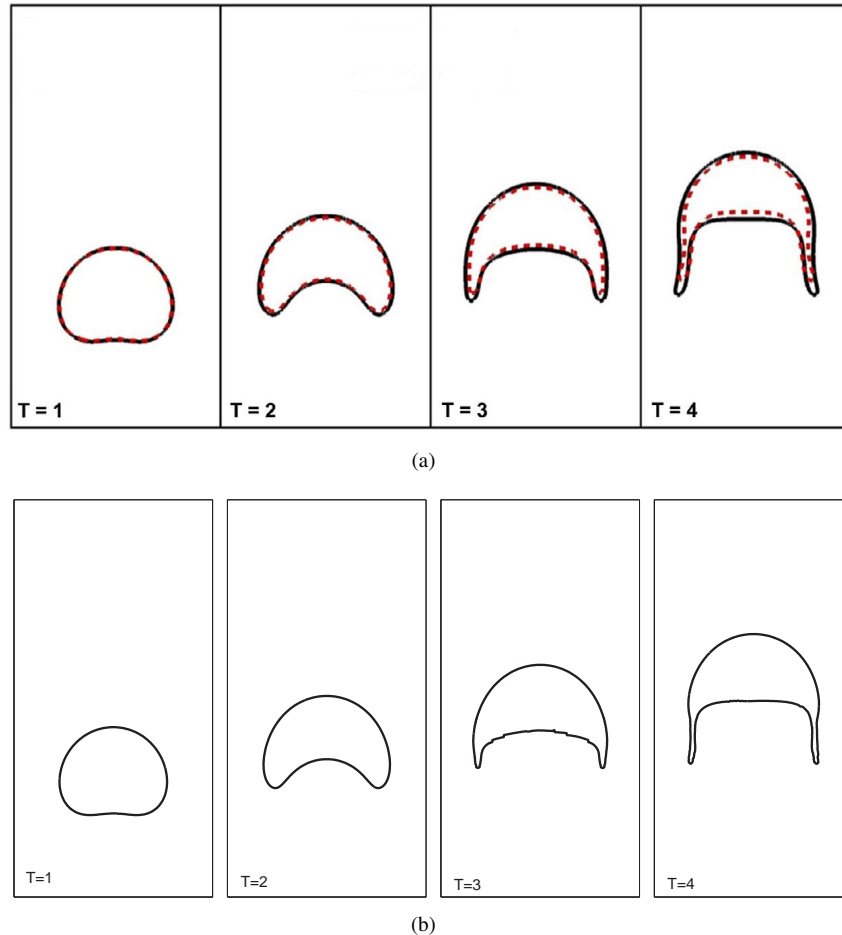


Fig. 4. Two-dimensional bubble dynamics with $Eo = 50$ and $Re = 35$, (a) the improved LB flux solver (Wang et al., 2015) and (b) the phase-field LBM (Su et al., 2018).

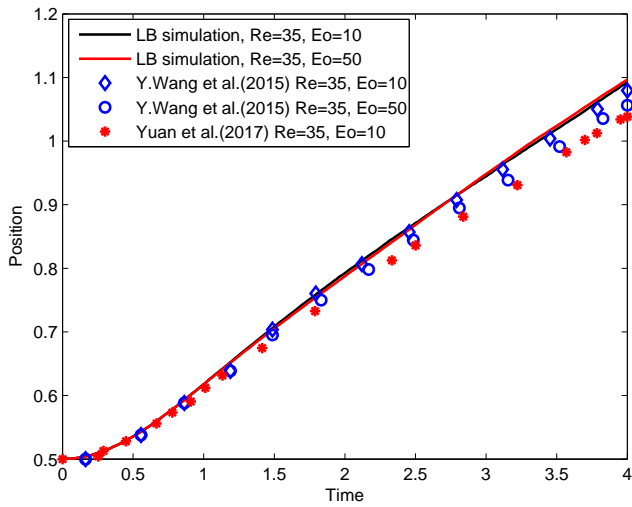


Fig. 5. Time evolution of position of the bubble mass center during the ascent with the density ratio $\rho_l/\rho_g = 1000$ (Su et al., 2018).

Using another improved phase-field-based LB model, Ren et al. (2016b) numerically studied a three-dimensional buoyancy-driven bubble rising with a small density ratio. Recently, based on the Allen-Cahn phase-field-based theory, Su et al. (2018)

proposed an advanced LB multiphase model for simulating multiphase flows with high density ratios and adopted it to investigate the single bubble rising dynamics at a large density ratio of 1000. The results of a two-dimensional bubble dynamics with $Eo = 50$ and $Re = 35$ are plotted in Fig. 4, where the numerical results of an improved LB flux solver is also presented (Wang et al., 2015). As seen from Fig. 4, the results of the phase-field based LB model qualitatively agree with those of LB flux solver. Further, the time evolution of position of the bubble mass center during the ascent is measured in Fig. 5, and we can observe that the numerical results are quantitatively consistent with the solutions of the improved LB flux solver (Wang et al., 2015) and the advanced LSM (Yuan et al., 2017). Liang et al. (2019a) also used a robust phase-field-based axisymmetric LB model to simulate the three-dimensional bubble rising dynamics with high density ratio. The simulation results with a wide range of the dimensionless Eötvös number and Morton number are shown in Table 1 (Liang et al., 2019a). For comparisons, the previous results including the experimental data (Bhaga and Weber, 1981), the front tracking simulation results of Hua and Lou (2007), and the numerical results of the axisymmetric LB model by Huang et al. (2014) are also presented. It is found that the results of phase-field-based LB model are qualitatively consistent with

Table 1. Comparison of terminal bubble shapes observed in experiments and predicted by the front tracking method, the previous phase-field LB simulation and an improved phase-field LBM (Liang et al., 2019a).

Case	experiments Bhaga et al., 1981	Hua et al., 2007	Huang et al., 2014	Liang et al., 2019a
A1				
A2				
A3				
A4				
A5				
A6				

the former two available data in general, and slightly deviate from the previous LB simulations.

4.3 The Rayleigh-Taylor instability

The Rayleigh-Taylor instability occurs whenever a heavier fluid is accelerated against a lighter one in the presence of a slight perturbation at the interface. It plays a key role in many different areas such as astrophysics, inertial confinement fusion, sprays, etc. Due to its wide applications, the Rayleigh-Taylor instability has been extensively studied using experimental, theoretical, and as well as numerical approaches (Zhou, 2017a; Zhou, 2017b). Several researchers have also used the phase-field-based LBM to study the Rayleigh-Taylor instability (He et al., 1999a; He et al., 1999b; Zu and He, 2013; Liang et al., 2014; Shao et al., 2014; Ren et al., 2016b), while the most of these work are only to validate the codes of the developed LB models. Two important physical quantities characterizing the Rayleigh-Taylor instability are the dimensionless Reynolds number and the Atwood number, which can be defined respectively as,

$$Re = \lambda \sqrt{A_t g \lambda / (1 + A_t)} / v, \quad A_t = \frac{\rho_l - \rho_g}{\rho_l + \rho_g}, \quad (87)$$

where λ is the characteristic length, g is the gravitational acceleration, and ρ_l, ρ_g represent the densities of the heavier and lighter fluids. He et al. (1999a) performed the earliest study of the Rayleigh-Taylor instability using the phase-field-based LB model. They examined the effects of the Reynolds and Atwood numbers, and reported that the model can successfully reproduce the complex interfacial dynamic behaviour in the evolution of the Rayleigh-Taylor instability. Later, He et al.

(1999b) also applied this LB scheme to investigate the three-dimensional Rayleigh-Taylor instability, and mainly focused on the evolution of the three-dimensional structure of the interface. Liang et al. (2014) used a Cahn-Hilliard phase-field based LB model to simulate the two-dimensional Rayleigh-Taylor instability, and analyzed the effect of the Reynolds number. Fig. 6 depicts the evolution of the Rayleigh-Taylor instability at four different Reynolds numbers. For a high Re , the roll-up behavior of the interface can be observed at the early time. The interface at the late time undergoes a chaotic breakup which induces the formation of an abundant of small dissociative droplets in the system. While for a low Re , the phase interface become stable and no vortices are observed in the whole process as the shear layer between the bubble and spike is stabilized due to the larger viscosity effect. Liang et al. (2016b) also adopted the phase-field-based LB model to investigate the three-dimensional Rayleigh-Taylor instability in a long square duct, and considered the effect of Reynolds number on the late-time interfacial dynamics and bubble amplitude. Fig. 7 shows the time evolution of the density contour in the immiscible Rayleigh-Taylor instability with four typical Reynolds numbers. The two-phase system at a high Reynolds number is unstable, and the phase interface undergoes a dramatic deformation at the multiple layers and some of them even have a chaotic breakup, leading to the formation of numerous small dissociative drops. As the Reynolds number is reduced, the structure of the interface becomes relatively smoothed and no breakup situations appear in the evolutional process. Fig. 8 depicts the normalized bubble amplitudes and velocities at several Reynolds numbers. From this figure, Liang et al. (2016b) recognized that the development of high-Reynolds-number Rayleigh-Taylor instability

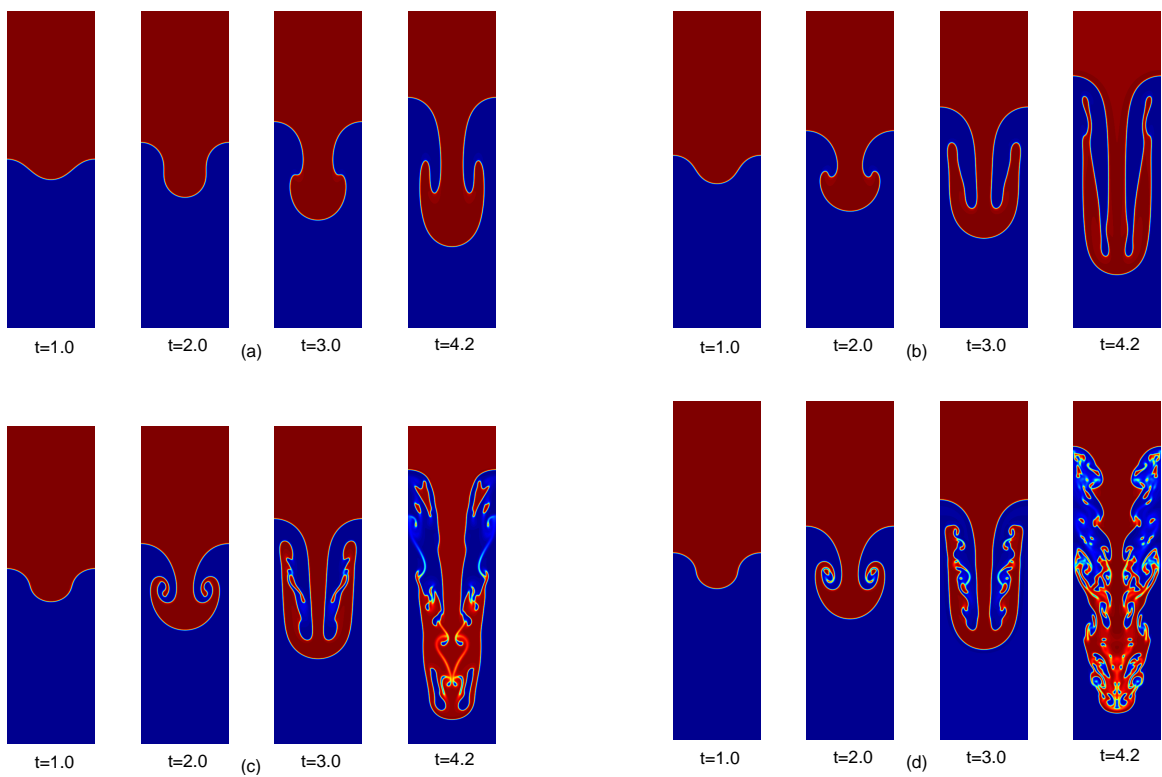
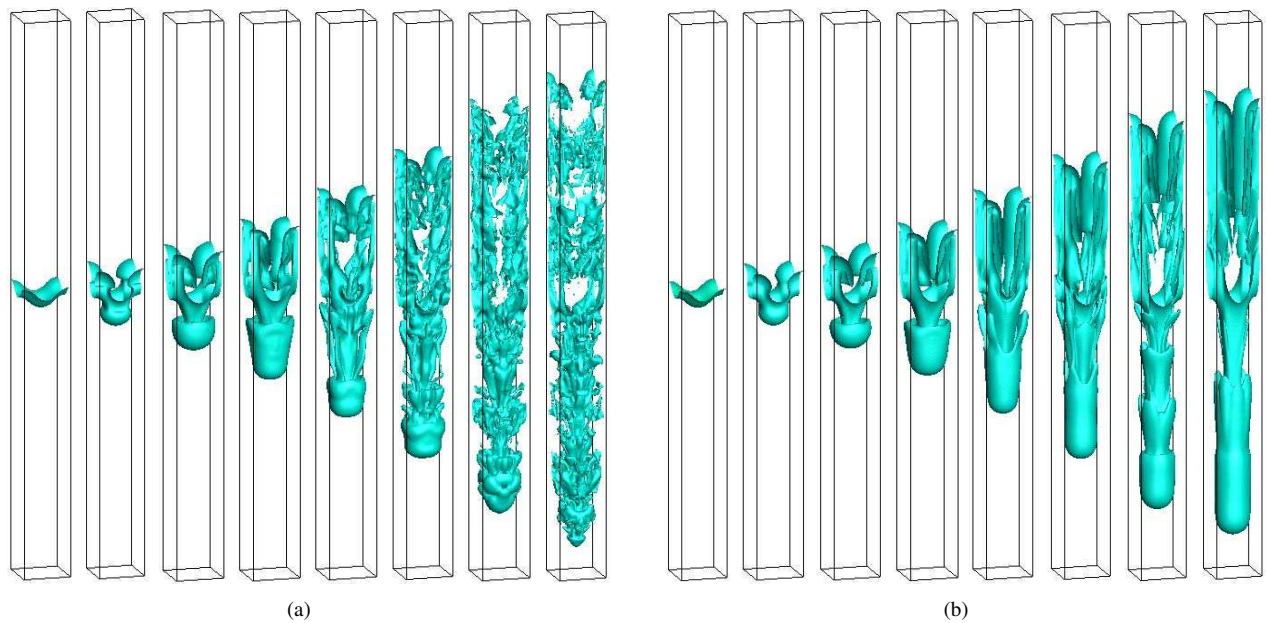


Fig. 6. Evolution of the density contours in immiscible Rayleigh-Taylor instability at various Reynolds numbers, (a) $Re = 30$, (b) $Re = 150$, (c) $Re = 3000$, (d) $Re = 30000$ (Liang et al., 2014).



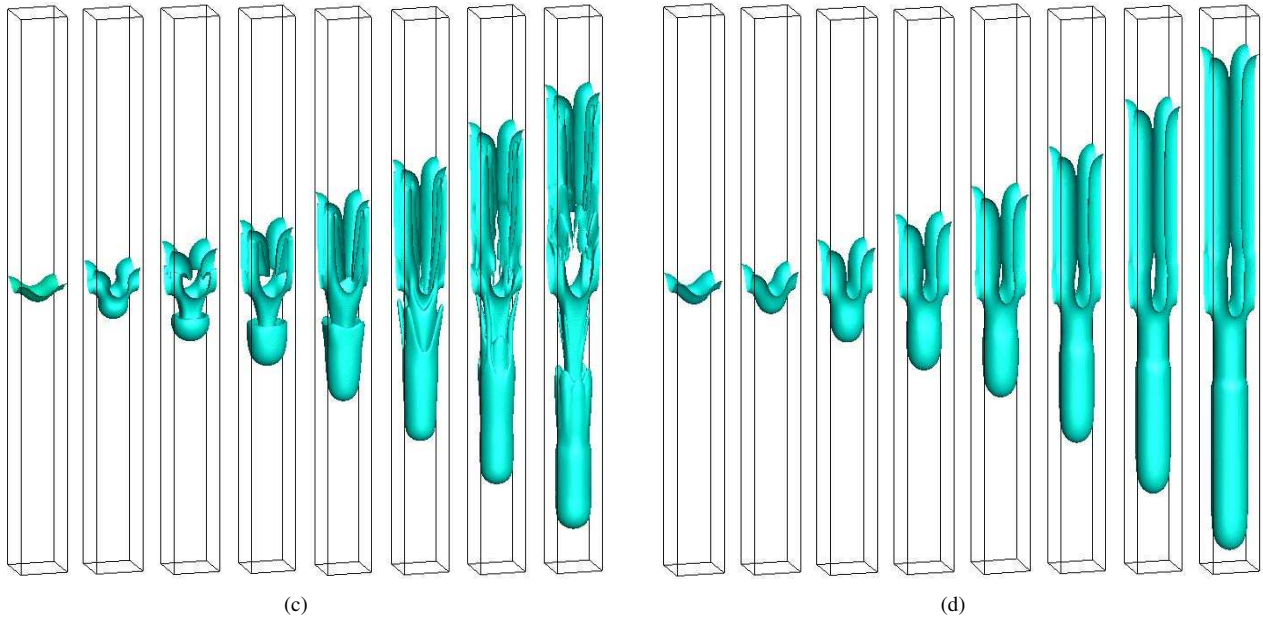


Fig. 7. Evolution of the density contours in the three-dimensional immiscible Rayleigh-Taylor instability at various Reynolds numbers, (a) $Re = 5000$, (b) $Re = 1000$, (c) $Re = 500$, and (d) $Re = 10$ (Liang et al., 2016b).

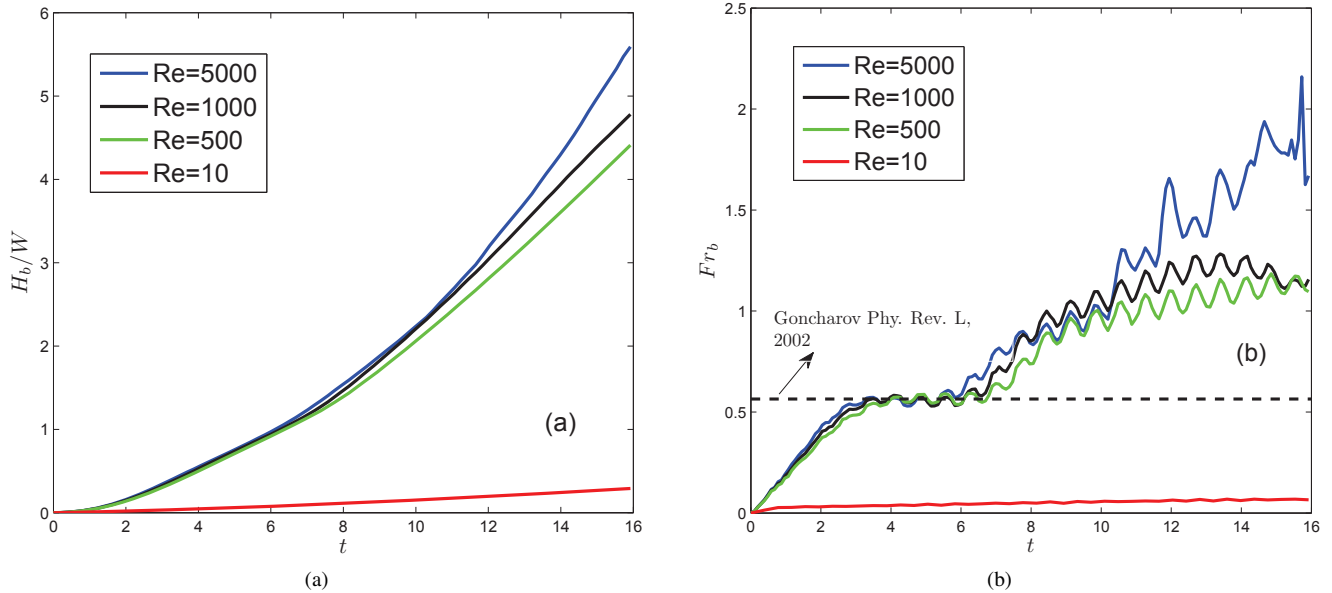


Fig. 8. Effect of Reynolds number on (a) normalized bubble amplitude and (b) normalized bubble velocity. The dashed line represents the analytical solution of the classic potential flow model (Goncharov et al., 2002).

with a low Atwood number experiences a sequence of stages, which includes the linear growth, terminal velocity growth, reacceleration and chaotic development stages. The bubble Froude number at the second stage shows a good agreement with the solution of the potential flow theory (Goncharov, 2002). The late-time bubble Froude number becomes unstable and fluctuates with the time, which suggests that the evolution of the instability has transformed to the chaotic stage. We also measured the bubble acceleration and present the results in Fig. 9. The normalized acceleration at late time fluctuates around a constant value of 0.16, indicating that the instability undergoes a mean quadric growth.

4.4 The droplet impact dynamics

Droplet impact on liquid or dry surfaces is a familiar spectacle in natural event of falling raindrop on the wet ground or puddle, and it also has great relevance to many technical applications, such as ink jet printing, spray cooling and coating. In spite of its ubiquity and extensive researches, numerical simulation of such flows still poses some challenges due to complex interfacial changes in topology, and yet there exists a large density difference for a water-air system. Further, a numerical singularity may be produced at the impact point. Lee and Lin (2005) proposed a large-density-ratio LB model

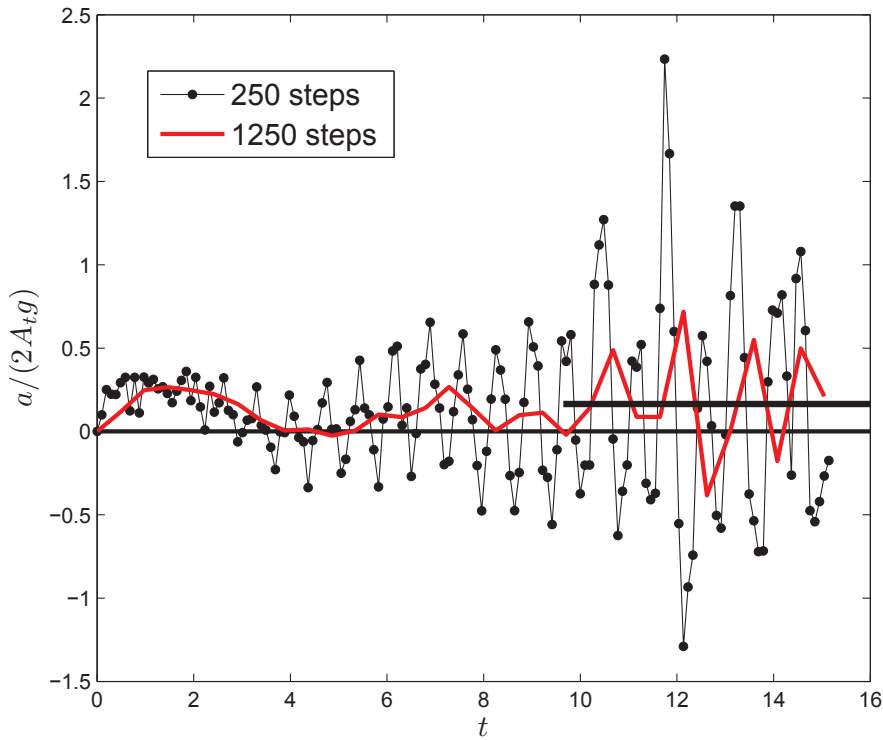


Fig. 9. Normalized bubble acceleration at a high Reynolds number. The solid line represents a constant value of 0.16 (Liang et al., 2016b).

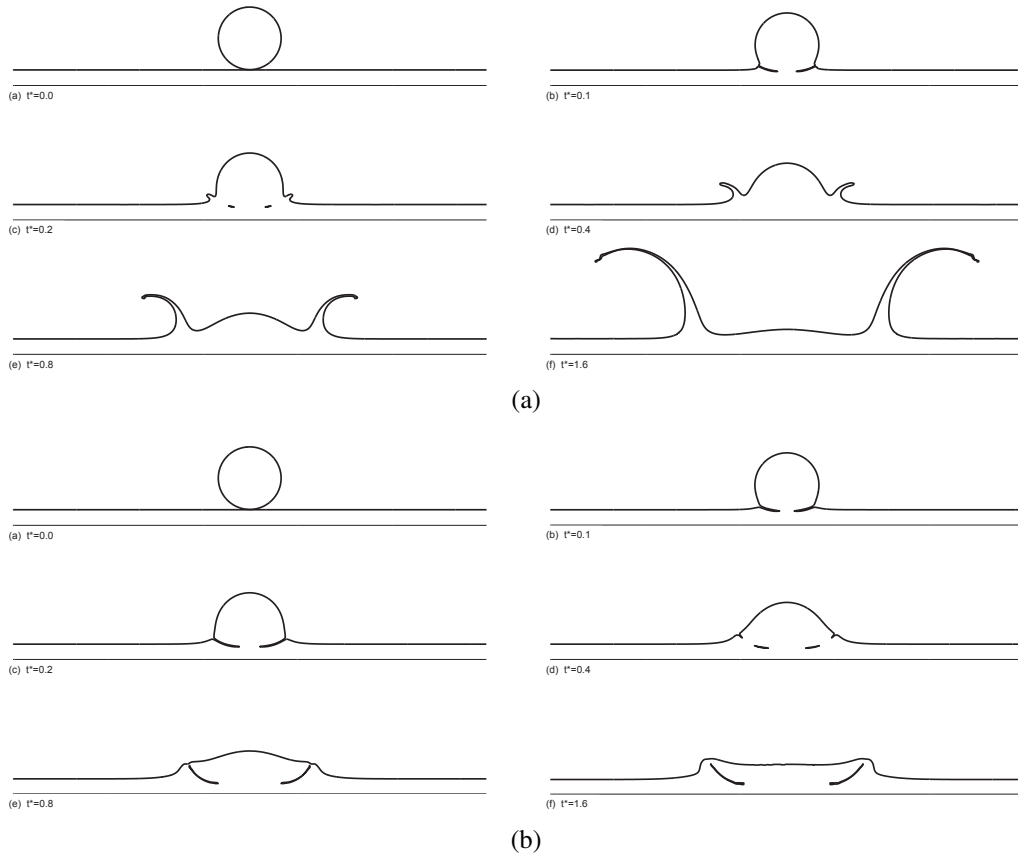


Fig. 10. Snapshots of droplet impact on a thin liquid film with (a) $Re = 500$ and (b) $Re = 20$, $We = 8000$, $\rho_l/\rho_g = 1000$ (Liang et al., 2018).

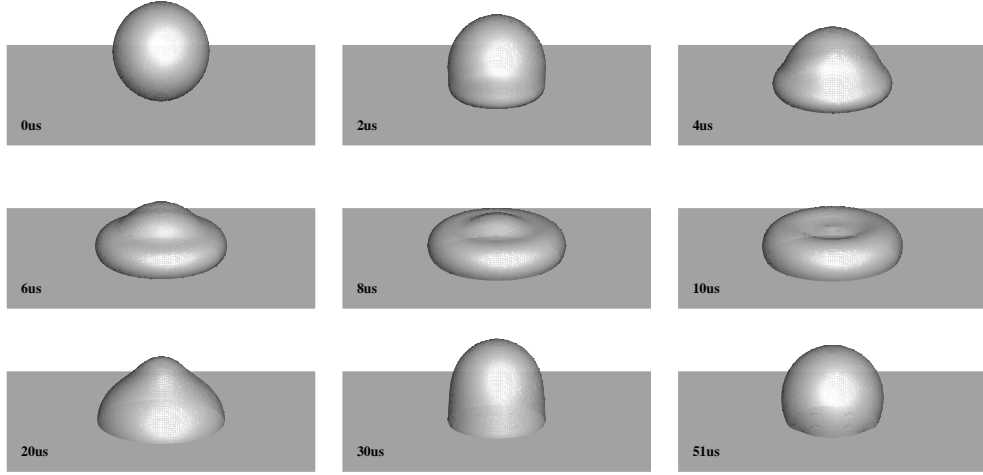


Fig. 11. Snapshots of micro-scale droplet impact on solid surface obtained by the LBM coupled with the geometrical wetting scheme, $\theta = 107^\circ$, $\rho_l/\rho_g = 844$ and $\mu_l/\mu_g = 48.5$ (Liang et al., 2019b).

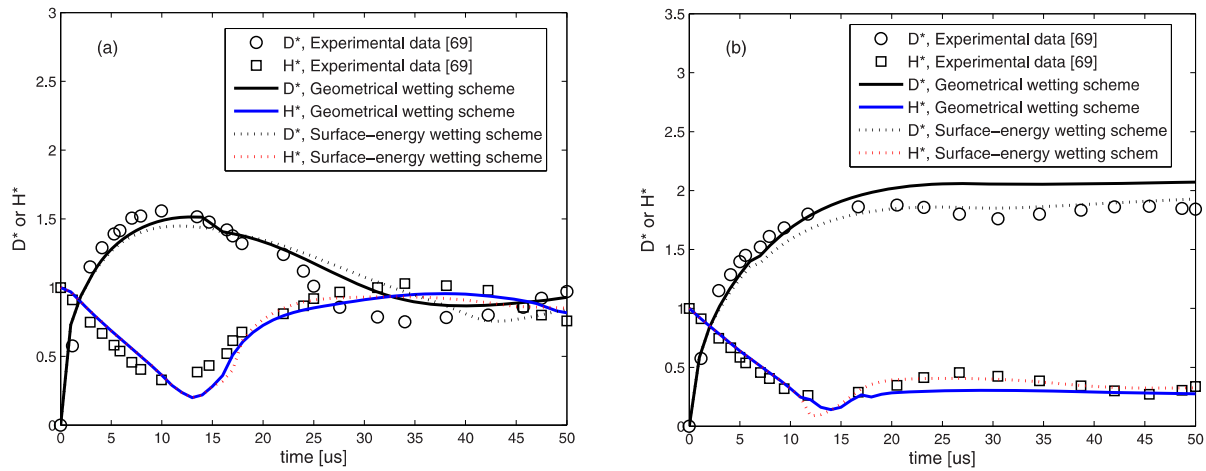


Fig. 12. The time evolutions of the spreading ratio D^* and dimensionless droplet height H^* obtained by the phase field lattice Boltzmann method coupled with surface-energy and geometrical wetting schemes from the left to the right, $\theta = 107^\circ$ and $\theta = 31^\circ$ (Liang et al., 2019b).

for two-phase flows from the phase-field viewpoint, and applied the model to simulate the droplet impact on the liquid and dry surfaces. The contribution to achieving a large density ratio is the use of a stable mixed difference scheme for computing gradient terms, while it leads to the slight violation of mass conservation. Fakhari et al. (2010) used a phase-field-based LB model to study the droplet impact on a liquid film with a small density ratio. Shao et al. (2014) adopted a modified phase-field-based LB model to simulate the droplet impact on a liquid film with a density ratio of 5. Liang et al. (2018) used another phase-field-based LB model to simulate the impact of a two-dimensional droplet on a liquid film with a high density ratio of 1000. Fig. 10 shows typical scenic representations of droplet impact processes at two different Reynolds numbers of 500 and 20. The fascinating phenomena of droplet splashing is successfully reproduced at a high Reynolds number, while the initial droplet only merges with the thin liquid film without the appearance of the splashing behavior at a low Reynolds number. They also reported that the measured spreading radius

in the simulation exhibits to obey the power-law relation. Liang et al. (2019b) further incorporated two popular contact angle models of the cubic surface-energy and geometrical schemes into the phase-field LBM and then applied it to study a three-dimensional micron-scale droplet impact on solid surface with a high density ratio. They found that the LBM can obtain the accurate results in predicting droplet patterns. Fig. 11 presents several typical snapshots of the micron-scale droplet impact processes at the contact angles of 107° . The micron-scale droplet instantly impacts on the substrate surface and then takes place of the rebounding. Finally, it undergoes a slight oscillation until reaching the equilibrium shape. The numerically predicted droplet impact dynamics are consistent with the experimental results (Dong et al., 2007). The droplet spreading radius and height in the impact processes are measured, and the time variations of these physical quantities with the contact angles of 107° and 31° are plotted in Fig. 12. For comparisons, the experimental results of Dong et al. (2007) are also presented. As shown in this figure,

the surface-energy and geometrical wetting schemes (Ding and Spelt, 2007) can obtain the comparative results, both of which are in good agreements with the experimental data in general.

5. Summary

In this paper, we present a brief review on the phase-field-based LBM for multiphase flows. Although the phase-field-based LBM has gained great success in the study of the complex multiphase flows, there are still some problems needed to be considered in the future. First of all, most of the work on the phase-field LBM are limited to two-phase flows, and the phase-field-based LB models for multiphase (more than three phases) flows are still in progress (Liang et al., 2016; Abadi et al., 2018; Zheng et al., 2019). Secondly, almost all of phase-field-based LB models are only suitable for isothermal multiphase flows, and it is desirable to develop the phase-field-based LB models for the non-isothermal multiphase flows (Liu et al., 2013; Zheng et al., 2016; Wang, 2018; Hu et al., 2019b), and finally, more advanced phase-field-based LB models for multiphase flows with surfactants and multiphase electrohydrodynamic flows are also needed (Liu and Zhang, 2010; Liu et al., 2019).

Acknowledgements

This work was financially supported by the National Natural Science Foundation of China (Grants No. 51576079, No. 51836003, No. 11602075 and No. 11972142) and the National Key Research and Development Program of China (Grant No. 2017YFE0100100).

Conflict of interest

The authors declare no competing interest.

Open Access This article is distributed under the terms and conditions of the Creative Commons Attribution (CC BY-NC-ND) license, which permits unrestricted use, distribution, and reproduction in any medium, provided the original work is properly cited.

References

- Abadi, R.H., Rahimian, M.H., Fakhari, A. Conservative phase-field lattice-Boltzmann model for ternary fluids. *J. Comput. Phys.* 2018, 374: 668-691.
- Aidun, C.K., Clausen, J.R. Lattice-Boltzmann method for complex flows. *Annu. Rev. Fluid Mech.* 2010, 42: 439-472.
- Allen, S., Cahn, J. Mechanisms of phase transformations within the miscibility gap of Fe-rich Fe-Al alloys. *Acta Metall.* 1976, 24(5): 425-437.
- Amaya-Bower, L., Lee, T. Single bubble rising dynamics for moderate Reynolds number using lattice Boltzmann method. *Comput. Fluids* 2010, 39(7): 1191-1207.
- Anderson, D.M., McFadden, G.B., Wheeler, A.A. Diffuse-interface methods in fluid mechanics. *Annu. Rev. Fluid Mech.* 1998, 30(1): 139-165.
- Anna, S. Droplets and bubbles in microfluidic devices. *Annu. Rev. Fluid Mech.* 2016, 48: 285-309.
- Bandalassi, V.E., Ceniceros, H.D., Banerjee, S. Computation of multiphase systems with phase field models. *J. Comput. Phys.* 2003, 190: 371-397.
- Bhaga, D., Weber, M.E. Bubbles in viscous liquids: shapes, wakes and velocities. *J. Fluid Mech.* 1981, 105: 61-85.
- Bonhomme, R., Magnaudet, J., Duval, F., et al. Inertial dynamics of air bubbles crossing a horizontal fluid-fluid interface. *J. Fluid Mech.* 2012, 707: 405-443.
- Brassel, M., Bretin, E. A modified phase field approximation for mean curvature flow with conservation of the volume. *Math. Meth. Appl. Sci.* 2011, 34: 1157-1180.
- Brennen, C.E. Fundamentals of multiphase flow. Cambridge university press, 2005.
- Cahn, J.W., Hilliard, J.E. Free energy of a nonuniform system. I. Interfacial free energy. *J. Chem. Phys.* 1958, 28(2): 258-267.
- Cahn, J.W., Hilliard, J.E. Free energy of a nonuniform system. III. Nucleation in a two-component incompressible fluid. *J. Chem. Phys.* 1959, 31(3): 688-699.
- Chai, Z., He, N., Guo, Z., et al. Lattice Boltzmann model for high-order nonlinear partial differential equations. *Phys. Rev. E* 2018a, 97: 013304.
- Chai, Z., Liang, H., Du, R., et al. A lattice Boltzmann model for two-phase flow in porous media. *SIAM J. Sci. Comput.* 2019, 41: B746-B772.
- Chai, Z., Shi, B., Guo, Z. A multiple-relaxation-time lattice Boltzmann model for general nonlinear anisotropic convection-diffusion equations. *J. Sci. Comput.* 2016, 69(1): 355-390.
- Chai, Z., Sun, D., Wang, H., et al. A comparative study of local and nonlocal Allen-Cahn equations with mass conservation. *Int. J. Heat Mass Transf.* 2018b, 122: 631-642.
- Chai, Z., Zhao, T. Effect of the forcing term in the multiple-relaxation-time lattice Boltzmann equation on the shear stress or the strain rate tensor. *Phys. Rev. E* 2002, 66: 016705.
- Chen, L., Kang, Q., Mu, Y., et al. A critical review of the pseudopotential multiphase lattice Boltzmann model: Methods and applications. *Int. J. Heat Mass Transf.* 2014, 76: 210-236.
- Chen, X., Hu G. Multiphase flow in microfluidic devices. *Adv. Appl. Mech.* 2015, 45: 201503.
- Chiu, P.H., Lin, Y.T. A conservative phase field method for solving incompressible two-phase flows. *J. Comput. Phys.* 2011, 230(1): 185-204.
- Chopard, B., Falcone, J.L., Latt, J. The lattice Boltzmann advection-diffusion model revisited. *Eur. Phys. J. Spec. Top.* 2009, 171(1): 245-249.
- Cristini, V., Tan, Y. Theory and numerical simulation of droplet dynamics in complex flows-a review. *Lab Chip* 2004, 4(4): 257-264.
- d'Humieres, D. Generalized lattice-Boltzmann equations. in: B.D. Shizgal, D.P. Weave (Eds.), *Rarefied Gas Dynamics: Theory and Simulations*, Prog. Astronaut. Aeronaut., vol. 159, AIAA, Washington, DC, 1992, pp. 450-458.
- Ding, H., Spelt, P.D., Shu, C. Diffuse interface model for incompressible two-phase flows with large density ratios.

- J. Comput. Phys. 2007, 226(2): 2078-2095.
- Ding, H., Spelt, P.D.M. Wetting condition in diffuse interface simulations of contact line motion. Phys. Rev. E 2007, 75(4): 046708.
- Dong, H., Carr, W.W., Bucknall, D.G., et al. Temporally-resolved inkjet drop impaction on surfaces. AIChE J. 2007, 53(10): 2606-2617.
- Fakhari, A., Geier, M., Bolster, D. A simple phase-field model for interface tracking in three dimensions. Comput. Math. Appl. 2016a, 78(4): 1154-1165.
- Fakhari, A., Geier, M., Lee, T. A mass-conserving lattice Boltzmann method with dynamic grid refinement for immiscible two-phase flows. J. Comput. Phys. 2016b, 315: 434-457.
- Fakhari, A., Rahimian, M.H. Phase-field modeling by the method of lattice Boltzmann equations. Phys. Rev. E 2010, 81(3): 036707.
- Folch, R., Casademunt, J., Hernández-Machado, A. Phase-field model for Hele-Shaw flows with arbitrary viscosity contrast. I. Theoretical approach. Phys. Rev. E 1999, 60: 1724-1733.
- Gan, H., Shan, X., Eriksson, T., et al. Reduction of droplet volume by controlling actuating waveforms in inkjet printing for micro-pattern formation. J. Micromech. Microeng. 2009, 19(5): 055010.
- Geier, M., Fakhari, A., Lee, T. Conservative phase-field lattice Boltzmann model for interface tracking equation. Phys. Rev. E 2015, 91(6): 063309.
- Goncharov, V.N. Analytical model of nonlinear, single-mode, classical Rayleigh-Taylor instability at arbitrary Atwood numbers. Phys. Rev. Lett. 2002, 88(13): 134502.
- Gunstensen, A.K., Rothman, D.H., Zaleski, S., et al. Lattice Boltzmann model of immiscible fluids. Phys. Rev. A 1991, 43(8): 4320.
- Guo, Z., Shi, B., Wang, N. Lattice BGK model for incompressible Navier-Stokes equation. J. Comput. Phys. 2000, 165(1): 288-306.
- Guo, Z., Shu, C. Lattice Boltzmann method and its applications in engineering. Singapore: World Scientific, 2013.
- Guo, Z., Zheng, C., Shi, B. Lattice Boltzmann equation with multiple effective relaxation times for gaseous microscale flow. Phys. Rev. E 2008, 77: 036707.
- Guo, Z., Zheng, C., Shi, B. Force imbalance in lattice Boltzmann equation for two-phase flows. Phys. Rev. E 2011, 83(3): 036707.
- He, X., Chen, S., Zhang, R. A lattice Boltzmann scheme for incompressible multiphase flow and its application in simulation of Rayleigh-Taylor instability. J. Comput. Phys. 1999a, 152(2): 642-663.
- He, X., Zhang, R., Chen, S., et al. On the three-dimensional Rayleigh-Taylor instability. Phys. Fluids 1999b, 11(5): 1143-1152.
- Hirt, C.W., Nichols, B.D. Volume of fluid (VOF) method for the dynamics of free boundaries. J. Comput. Phys. 1981, 39(1): 201-225.
- Hohenberg, P.C., Halperin, B.I. Theory of dynamic critical phenomena. Rev. Mod. Phys. 1977, 49(3): 435.
- Hu, Y., Li, D., Jin, L., et al. Hybrid Allen-Cahn-based lattice Boltzmann model for incompressible two-phase flows: The reduction of numerical dispersion. Phys. Rev. E 2019a, 99(2): 023302.
- Hu, Y., Li, D., Niu, X., et al. A diffuse interface lattice Boltzmann model for thermocapillary flows with large density ratio and thermophysical parameters contrasts. Int. J. Heat Mass Transf. 2019b, 138: 809-824.
- Hua, J., Lin, P., Liu, C., et al. Energy law preserving C0 finite element schemes for phase field models in two-phase flow computations. J. Comput. Phys. 2011, 230(19): 7115-7131.
- Hua, J., Lou, J. Numerical simulation of bubble rising in viscous liquid. J. Comput. Phys. 2007, 222: 769-795.
- Huang, H., Huang, J., Lu, Y. A mass-conserving axisymmetric multiphase lattice Boltzmann method and its application in simulation of bubble rising. J. Comput. Phys. 2014, 269: 386-402.
- Huang, H., Sukop, M., Lu, X. Multiphase lattice Boltzmann methods: Theory and application. John Wiley & Sons, 2015.
- Inamuro, T., Konishi, N., Ogino, F. A Galilean invariant model of the lattice Boltzmann method for multiphase fluid flows using free-energy approach. Comput. Phys. Commun. 2000, 129(1-3): 32-45.
- Jacqmin, D. Calculation of two-phase Navier-Stokes flows using phase-field modeling. J. Comput. Phys. 1999, 155(1): 96-127.
- Jullien, M., Tsang, M., Cohen, C., et al. Droplet breakup in microfluidic T-junctions at small capillary numbers. Phys. Fluids 2009, 21(7): 072001.
- Kendon, V.M., Cates, M.E., Pagonabarraga, I., et al., Inertial effects in three-dimensional spinodal decomposition of a symmetric binary fluid mixture: A lattice Boltzmann study. J. Fluid Mech. 2001, 440: 147-203.
- Kim, J., Lee, S., Choi, Y. A conservative Allen-Cahn equation with a space Ctime dependent Lagrange multiplier. Int. J. Eng. Sci. 2014, 84: 11-17.
- Kim, J., Jeong, D., Yang, S.D., et al. A finite difference method for a conservative Allen-Cahn equation on non-flat surfaces. J. Comput. Phys. 2017, 334: 170-181.
- Kintses, B., Van Vliet, L., Devenish, S., et al. Microfluidic droplets: New integrated workflows for biological experiments. Curr. Opin. Chem. Biol. 2010, 14(5): 548-555.
- Krüger, T., Kusumaatmaja, H., Kuzmin, A., et al. The lattice Boltzmann method: Principles and practice. Springer, Switzerland, 2017.
- Kurtoglu, I.O., Lin, C.L. Lattice Boltzmann study of bubble dynamics. Numer. Heat Transf. B 2006, 50(4): 333-351.
- Lallemand, P., Luo, L.S. Theory of the lattice Boltzmann method: Dispersion, dissipation, isotropy, Galilean invariance, and stability. Phys. Rev. E 2000, 61(6): 6546.
- Lee, D., Kim, J. Comparison study of the conservative Allen-Cahn and the Cahn-Hilliard equations. Math. Comput. Simul. 2016, 119: 35-56.
- Lee, H., Kim, J. An efficient and accurate numerical algorithm for the vector-valued Allen-Cahn equations. Comput.

- Phys. Commun. 2012, 183: 2107-2115.
- Lee, T., Lin, C.L. A stable discretization of the lattice Boltzmann equation for simulation of incompressible two-phase flows at high density ratio. *J. Comput. Phys.* 2005, 206(1): 16-47.
- Leshansky, A., Afkhami, S., Jullien, M., et al. Obstructed breakup of slender drops in a microfluidic T junction. *Phys. Rev. Lett.* 2012, 108(26): 264502.
- Li, Q., Luo, K., Gao, Y., et al. Additional interfacial force in lattice Boltzmann models for incompressible multiphase flows. *Phys. Rev. E* 2012, 85(2): 026704.
- Li, Q., Luo, K., Kang, Q., et al. Lattice Boltzmann methods for multiphase flow and phase-change heat transfer. *Prog. Energy Combust. Sci.* 2016, 52: 62-105.
- Li, W., Vigil R.D., Beresnev I.A., et al. Vibration-induced mobilization of trapped oil ganglia in porous media: Experimental validation of a capillary-physics mechanism. *J. Colloid Interface Sci.* 2005, 289(1): 193-199.
- Liang H., Liu H., Chai Z., et al. Lattice Boltzmann method for contact-line motion of binary fluids with high density ratio. *Phys. Rev. E* 2019b, 99(6): 063306.
- Liang, H., Li, Q., Shi, B., et al. Lattice Boltzmann simulation of three-dimensional Rayleigh-Taylor instability. *Phys. Rev. E* 2016b, 93(3): 033113.
- Liang, H., Li, Y., Chen, J., et al. Axisymmetric lattice Boltzmann model for multiphase flows with large density ratio. *Int. J. Heat Mass Tran.* 2019a, 130: 1189-1205.
- Liang, H., Shi, B., Chai, Z. Lattice Boltzmann modeling of three-phase incompressible flows. *Phys. Rev. E* 2016a, 93(1): 013308.
- Liang, H., Shi, B., Chai, Z. An efficient phase-field-based multiple-relaxation-time lattice Boltzmann model for three-dimensional multiphase flows. *Comput. Math. Appl.* 2017, 73(7): 1524-1538.
- Liang, H., Shi, B., Guo Z., et al. Phase-field-based multiple-relaxation-time lattice Boltzmann model for incompressible multiphase flows, *Phys. Rev. E* 2014, 89: 053320.
- Liang, H., Xu, J., Chen, J., et al. Phase-field-based lattice Boltzmann modeling of large-density-ratio two-phase flows. *Phys. Rev. E* 2018, 97(3): 033309.
- Link, D., Anna, S., Weitz, D., et al. Geometrically mediated breakup of drops in microfluidic devices. *Phys. Rev. Lett.* 2004, 92(5): 054503.
- Liu, C., Shen, J. A phase field model for the mixture of two incompressible fluids and its approximation by a Fourier-spectral method. *Physica D* 2003, 179(3-4): 211-228.
- Liu, H., Kang, Q., Leonardi C.R., et al. Multiphase lattice Boltzmann simulations for porous media applications. *Comput. Geosci.* 2016, 20(4): 777-805.
- Liu, H., Valocchi, A.J., Zhang, Y., et al. Phase-field-based lattice Boltzmann finite-difference model for simulating thermocapillary flows. *Phys. Rev. E* 2013, 87(1): 013010.
- Liu, H., Valocchi, A.J., Zhang, Y., et al. Lattice Boltzmann phase-field modeling of thermocapillary flows in a confined microchannel. *J. Comput. Phys.* 2014, 256: 334-356.
- Liu, H., Zhang, Y. Phase-field modeling droplet dynamics with soluble surfactants. *J. Comput. Phys.* 2010, 229(24): 9166-9187.
- Liu, X., Chai, Z., Shi, B. A phase-field-based lattice Boltzmann modeling of two-phase electro-hydrodynamic flows. *Phys. Fluids* 2019, 31: 092103.
- Lou, Q., Guo, Z., Shi, B. Effects of force discretization on mass conservation in lattice Boltzmann equation for two-phase flows. *Europhys. Let.* 2012, 99(6): 64005.
- Lowengrub, J., Truskinovsky, L. Quasi-incompressible Cahn-CHilliard fluids and topological transitions. *P. Roy. Soc. A-Math. Phy.* 1998, 454(1978): 2617-2654.
- Muradoglu, M., Tasoglu, S. A front-tracking method for computational modeling of impact and spreading of viscous droplets on solid walls. *Comput. Fluids* 2010, 39(4): 615-625.
- Qian, Y.H., d'Humires, D., Lallemand, P. Lattice BGK models for Navier-Stokes equation. *Europhys. Let.* 1992, 17(6): 479.
- Ren, F., Song, B., Sukop, M.C., et al. Improved lattice Boltzmann modeling of binary flow based on the conservative Allen-Cahn equation. *Phys. Rev. E* 2016a, 94(2): 023311.
- Ren, F., Song, B., Sukop, M.C. Terminal shape and velocity of a rising bubble by phase-field-based incompressible lattice Boltzmann model. *Water Resour. Res.* 2016b, 97: 100-109.
- Rubinstein, J., Sternberg, P. Nonlocal reaction-diffusion equations and nucleation. *IMA J. Appl. Math.* 1992, 48(3): 249-264.
- Scarbolo, L., Molin, D., Perlekar, P., et al. Unified framework for a side-by-side comparison of different multicomponent algorithms: Lattice Boltzmann vs. phase field model. *J. Comput. Phys.* 2013, 234: 263-279.
- Shan, X., Chen, H. Lattice Boltzmann model for simulating flows with multiple phases and components. *Phys. Rev. E* 1993, 47(3): 1815.
- Shan, X., Chen, H. Simulation of nonideal gases and liquid-gas phase transitions by the lattice Boltzmann equation. *Phys. Rev. E* 1994, 49(4): 2941.
- Shao, J.Y., Shu, C., Huang, H.B., et al. Free-energy-based lattice Boltzmann model for the simulation of multiphase flows with density contrast. *Phys. Rev. E* 2014, 89(3): 033309.
- Shen, J. Modeling and numerical approximation of two-phase incompressible flows by a phase-field approach. *Multiscale Modeling And Analysis For Materials Simulation*, 2012.
- Shi, B., Deng, B., Du, R., et al. A new scheme for source term in LBGK model for convection-diffusion equation. *Comput. Math. Appl.* 2008, 55: 1568-1575.
- Shi, B., Guo, Z. Lattice Boltzmann model for nonlinear convection-diffusion equations. *Phys. Rev. E* 2009, 79(1): 016701.
- Smith, K.A., Solis, F.J., Chopp, D. A projection method for motion of triple junctions by level sets. *Interface. Free Bound.* 2002, 4(3): 263-276.
- Succi, S. The Lattice Boltzmann Equation for Fluid Dynamics and Beyond. Oxford: Clarendon Press, 2001.

- Sun, Y., Beckermann, C. Sharp interface tracking using the phase-field equation. *J. Comput. Phys.* 2007, 220(2): 626-653.
- Sussman, M., Smereka, P., Osher, S. A level set approach for computing solutions to incompressible two-phase flow. *J. Comput. Phys.* 1994, 114(1): 146-159.
- Sussman, M., Smith, K.M., Hussaini, M.Y., et al. A sharp interface method for incompressible two-phase flows. *J. Comput. Phys.* 2007, 221(2): 469-505.
- Su, T., Li, Y., Liang, H., et al. Numerical study of single bubble rising dynamics using the phase field lattice Boltzmann method. *Int. J. Mod. Phys. C* 2018, 29(11): 1-27.
- Swift, M.R., Osborn, W., Yeomans, J. Lattice Boltzmann simulation of nonideal fluids. *Phys. Rev. Lett.* 1995, 75(5): 830.
- Teh, S.Y., Lin, R., Hung, L.H., et al. Droplet microfluidics. *Lab Chip* 2008, 8(2): 198-220.
- Unverdi, S.O., Tryggvason, G. A front-tracking method for viscous, incompressible, multi-fluid flows. *J. Comput. Phys.* 1992, 100(1): 25-37.
- Wang, H., Chai, Z., Shi, B., et al. Comparative study of the lattice Boltzmann models for Allen-Cahn and Cahn-Hilliard equations. *Phys. Rev. E* 2016, 94(3): 033304.
- Wang, H. Phase-field lattice Boltzmann method for flow and heat transfer of multiphase fluid. Ph.D Thesis, Huazhong University of Science and Technology, 2018.
- Wang, Y., Shu, C., Shao, J.Y., et al. A mass-conserved diffuse interface method and its application for incompressible multiphase flows with large density ratio. *J. Comput. Phys.* 2015, 290: 336-351.
- Wörner, M. Numerical modeling of multiphase flows in microfluidics and microprocess engineering: A review of methods and applications. *Microfluid. Nanofluid.* 2012, 12(6): 841-886.
- Yang, K., Guo, Z. Lattice Boltzmann method for binary fluids based on mass-conserving quasi-incompressible phase-field theory. *Phys. Rev. E* 2016, 93(4): 043303.
- Yang, X., Forest, M.G., Li, H., et al. Modeling and simulations of drop pinch-off from liquid crystal filaments and the leaky liquid crystal faucet immersed in viscous fluids. *J. Comput. Phys.* 2013, 236: 1-14.
- Yuan, H.Z., Chen, Z., Shu, C., et al. A free energy-based surface tension force model for simulation of multiphase flows by level-set method. *J. Comput. Phys.* 2017, 345: 404-426.
- Yue, P., Feng, J., Liu, C., et al. A diffuse-interface method for simulating two-phase flows of complex fluids. *J. Fluid Mech.* 2004, 515: 293-317.
- Yue, P., Zhou, C., Feng, J. Spontaneous shrinkage of drops and mass conservation in phase-field simulations. *J. Comput. Phys.* 2007, 223(1): 1-9.
- Zhai, S., Weng, Z., Feng, X. Investigations on several numerical methods for the non-local Allen-Cahn equation. *Int. J. Heat Mass Transf.* 2015, 87: 111-118.
- Zhang, S., Wang, M. A nonconforming finite element method for the Cahn-Hilliard equation. *J. Comput. Phys.* 2010, 229(19): 7361-7372.
- Zheng, L., Zheng, S., Zhai, Q. Lattice Boltzmann equation method for the Cahn-Hilliard equation. *Phys. Rev. E* 2015, 91(1): 013309.
- Zheng, L., Zheng, S., Zhai, Q. Continuous surface force based lattice Boltzmann equation method for simulating thermocapillary flow. *Phys. Lett. A* 2016, 380(4): 596-603.
- Zheng, L., Zheng, S. Phase-field-theory-based lattice Boltzmann equation method for N immiscible incompressible fluids. *Phys. Rev. E* 2019, 99(6): 063310.
- Zheng, H., Shu, C., Chew, Y.T. Lattice Boltzmann interface capturing method for incompressible flows. *Phys. Rev. E* 2005, 72(5): 056705.
- Zheng, H., Shu, C., Chew, Y.T. A lattice Boltzmann model for multiphase flows with large density ratio. *J. Comput. Phys.* 2006, 218(1): 353-371.
- Zheng, H., Shu, C., Chew, Y.T., et al. Three-dimensional lattice Boltzmann interface capturing method for incompressible flows. *Int. J. Numer. Methods Fluids* 2008, 56(9): 1653-1671.
- Zhou, Y. Rayleigh-Taylor and Richtmyer-Meshkov instability induced flow, turbulence, and mixing. I. *Phys. Rep.* 2017a, 720: 1-136.
- Zhou, Y. Rayleigh-Taylor and Richtmyer-Meshkov instability induced flow, turbulence, and mixing. II. *Phys. Rep.* 2017b, 723: 1-160.
- Zu, Y., He, S. Phase-field-based lattice Boltzmann model for incompressible binary fluid systems with density and viscosity contrasts. *Phys. Rev. E* 2013, 87(4): 043301.